

Petrogenesis of the Dunite Peak ophiolite, south-central Yukon and the distinction of upper plate and lower plate settings: a new hypothesis for the late Paleozoic – early Mesozoic tectonic evolution of the Northern Cordillera

A.J. Parsons^{1*}, A. Zagorevski², J.J. Ryan¹, W.C. McClelland³, C.R. van Staal¹, M.J. Coleman⁴, M.L. Golding¹.

* *andrew.parsons@earth.ox.ac.uk*

¹*Dept. Earth Sciences, University of Oxford, South Parks Road, Oxford, OX1 3AN, United Kingdom.*

²*Geological Survey of Canada, 1500-605 Robson Street, Vancouver, BC, V6B5J, Canada.*

³*Geological Survey of Canada, 601 Booth St., Ottawa, ON, K1A 0E8, Canada.*

⁴*Dept. Earth and Environmental Sciences, 115 Trowbridge Hall, University of Iowa, Iowa City, IA, 52242, USA.*

⁵*Dept. Earth and Environmental Sciences, University of Ottawa, 120 University, Ottawa, ON. K1N 6N5, Canada.*

ABSTRACT

Upper plate and lower plate settings within subduction zones have distinct geological signatures. Identifying and discriminating between these settings is crucial to the study of accretionary orogens. We apply this distinction to the Northern Cordillera in Yukon, British Columbia and Alaska, and focus on the identification of upper plate and lower plate domains during the late Paleozoic to early Mesozoic evolution of the allochthonous Yukon-Tanana terrane, the west Laurentian margin and the intervening Slide Mountain Ocean. We present new data from the Dunite Peak ophiolite in south-central Yukon, previously interpreted as ocean plate stratigraphy that was obducted from the subducting Slide Mountain Ocean (i.e. lower plate). Whole-rock geochemical and Sm-Nd isotopic analyses, and U-Pb zircon geochronology indicate that the Dunite Peak ophiolite formed in an intra-oceanic suprasubduction zone setting (i.e. upper plate) with

magmatism at 265 ± 4 Ma. We propose that the Dunite Peak ophiolite correlates with other mid-Permian suprasubduction zone ophiolites of the Slide Mountain terrane, collectively defining the previously unrecognized mid-Permian *Dunite Peak intra-oceanic arc*. This intra-oceanic arc was active from ~280 to 260 Ma, located within the Slide Mountain Ocean, between the Yukon-Tanana terrane and west Laurentia. Existence of this arc is incompatible with previous models which proposed that accretion of the Yukon-Tanana terrane to Laurentia was facilitated by Permian subduction of Slide Mountain Ocean beneath the Yukon-Tanana terrane. Our results, combined with existing datasets suggest that during the mid- to late Permian, Yukon-Tanana terrane subducted eastward beneath the Dunite Peak intra-oceanic arc. Subsequent collision and accretion of the Yukon-Tanana – Dunite Peak composite terrane with Laurentia must have occurred after the Middle Triassic.

1. INTRODUCTION

The understanding of subduction, accretion and collision processes in active and ancient settings has been vastly improved by modern geochemical and geochronological constraints. Specifically, subduction zone upper-plate settings and subduction zone lower-plate settings in accretionary orogens may be discriminated using key geochemical indicators, especially with respect to the origin and timing of formation of ophiolites (e.g. Wilson, 1989; Wakabayashi & Dilek, 2000; Pearce, 2008, 2014; Dilek & Furnes, 2014; McGoldrick *et al.*, 2017). In this study, we investigate the petrogenesis of Permian ophiolites associated with the Slide Mountain terrane (SMT) of the Northern Cordillera accretionary orogen in Alaska, Yukon and British Columbia (Figure 1), with particular focus on distinction between subduction zone upper-plate and subduction zone lower-plate processes. This includes new field, geochemical and geochronological analyses of the Dunite Peak ophiolite (de Keijzer *et al.*, 2000; Parsons *et al.* 2017a, b) in south-central Yukon, which has been assigned previously to the SMT (e.g. Colpron *et al.*, 2016). Previous studies consider the SMT to be the accreted remnants of the Slide Mountain Ocean, which they interpreted as a back-arc oceanic basin between the western Laurentian margin and the allochthonous Yukon-Tanana terrane (YTT, a continental island arc), during the Late Devonian to Permian (see review of Nelson *et al.*, 2013).

In this study, we first present the concept of upper-plate and lower-plate distinctions in subduction zone settings and their relevance for studies of accretionary orogens. This is followed by an introduction to current tectonic models for the Northern Cordillera and the locally defined mid- to late Permian ‘*Klondike orogeny*’ (260-252.2 Ma) as proposed by previous works (e.g. Mortensen, 1992a; Beranek & Mortensen, 2011; Nelson *et al.*, 2006; 2013; Colpron *et al.*, 2006a; 2007). We present new data from the Dunite Peak ophiolite (Figure 1e), integrate it with existing data from the SMT, and argue that most mid-Permian ophiolites assigned to the SMT are supra-subduction zone (SSZ) ophiolites, derived from the upper plate of a previously unrecognized intra-oceanic arc. We define this arc as the *Dunite Peak intra-oceanic arc*.

Our findings are incompatible with current tectonic models for Northern Cordillera and require an alternative explanation. We integrate our findings with existing datasets to present a new hypothesis for the late Paleozoic to early Mesozoic evolution of the Northern Cordillera. This study not only bears significance

for our understanding of the Northern Cordillera, but also demonstrates the importance of identifying and distinguishing between upper-plate and lower-plate components in any accretionary orogen, and how misidentification of such components can result in markedly different tectonic interpretations.

1.1. Upper plate – lower plate distinction in accretionary orogens

Distinguishing subduction zone upper-plate processes/components from subduction zone lower-plate processes/components is a complicated and yet essential part of any study of accretionary orogens (e.g. Wakabayashi & Dilek, 2000; Zagorevski & van Staal, 2011; McGoldrick *et al.*, 2017). Here, we define *accretion* as the sequential addition of material from a subducting lower plate to an overriding upper plate or vice versa, via underplating obduction or transform faulting. We define the term *collision* as entry of a lower plate oceanic plateau, arc or continental lithosphere into a subduction zone. During the life of an active subduction zone, it is possible to classify the structural components that interact with it into one of three groups: (1) Upper-plate material of the active subduction zone. These include the arc, fore-arc and back-arc, plus the arc substrate comprising continental lithosphere, oceanic lithosphere or fragments of the two. Where oceanic lithosphere is present in the upper plate, SSZ ophiolites may also form in this setting (e.g. Dilek & Furnes, 2014). (2) Subducted lower-plate material. This group accounts for almost all lower-plate oceanic lithosphere that enters a subduction zone and is rarely preserved in the geological record as most of this material subducts into the mantle (e.g. Dewey, 2003; Wakabayashi, 2017). At the point of cessation of subduction, this lower-plate material may be preserved, juxtaposed to the upper plate via a suture. In such cases, cessation of subduction typically corresponds to a collision, facilitated by the arrival of a lower-plate arc, continent, or ocean plateau into the subduction zone (e.g. Cloos, 1993; Mann & Taira, 2004; Afonso & Zlotnik, 2011; Brown *et al.*, 2011). (3) Accreted lower-plate material. Material derived from the lower plate that is accreted to the upper plate during subduction-accretion (e.g. the Franciscan complex, California; Wakabayashi, 2017). For ancient subduction zones this is usually the only remaining record of the lower plate and is commonly used to reconstruct the paleo-ocean plate stratigraphy of the lower plate (e.g. Isozaki *et al.*, 1990; Kusky *et al.*, 2013; Wakabayashi, 2017).

Distinguishing between upper-plate and accreted lower-plate material may be challenging in any subduction zone setting, but is particularly difficult when studying polyphase accretionary orogens such as the Central Asian orogenic belt (e.g. Lin *et al.*, 2018), the Appalachians (e.g. van Staal *et al.*, 2009; Zagorevski & van Staal, 2011) or the Northern Cordillera (e.g. Nelson *et al.*, 2013). Such orogens preserve episodic collisions, formation of composite terranes, and subduction polarity reversals, which result in upper- and lower-plate material of older subduction zones (including SSZ ophiolites) residing in either the lower or upper plates of a younger subduction zone (e.g. Lush's Bight ophiolite, Newfoundland, Zagorevski & van Staal, 2011). In such settings, the study of ophiolites and accretionary complexes can provide an invaluable record of subduction-accretion and paleo-subduction polarity during multiple collisional and suturing events (e.g. Dilek & Furnes, 2014; Zagorevski & van Staal, 2011; Wakabayashi, 2017). However, misidentification of upper-plate, accreted lower-plate and subducted lower-plate material in an accretionary orogen can lead to unlikely or implausible tectonic models, as is discussed below (*section 2*).

2. THE NORTHERN CORDILLERA AND THE KLONDIKE OROGENY (PREVIOUS WORK)

The North American Cordillera accretionary orogen (Figure 1) has served as a type example for accretionary orogenesis since the establishment of the terrane concept (Coney *et al.*, 1980). It has a complex tectonic evolution that involved multiple extensional, collisional and magmatic events since the Proterozoic, followed by as much as 1000-2000 km lateral displacement of accreted allochthonous and parautochthonous units during the Cenozoic (see review of Nelson *et al.*, 2013). This study focuses on the Paleozoic-Mesozoic accretionary history of YTT, SMT and the Laurentian margin, which occurred prior to Mesozoic to Eocene dextral translation of terranes along the Cordilleran margin (e.g. Gabrielse *et al.*, 2006).

It is generally accepted that YTT is an allochthonous continental island arc terrane (Figure 1) built on a substrate of peri-cratonic (Laurentian) continental crust (e.g. Colpron *et al.*, 2006a; Piercey & Colpron, 2009; Nelson *et al.*, 2013). The SMT (Figure 1) comprises Mississippian to early Permian supracrustal igneous and sedimentary oceanic rocks and mid-Permian mafic-ultramafic ophiolites that are interpreted as vestiges of accreted ocean floor stratigraphy of the Slide Mountain Ocean (see summaries by Nelson *et al.*,

2006, 2013). Most models propose that YTT rifted from the west margin of the Laurentia during the Late Devonian – Early Mississippian via back-arc rifting of the Yukon-Tanana arc to form the Slide Mountain Ocean (e.g. Mortensen, 1992a; Nelson *et al.*, 2006; 2013; Colpron *et al.*, 2006a, 2007). These models then propose a subduction polarity reversal across YTT from east-dipping subduction of the Panthalassa Ocean to west-dipping subduction of the Slide Mountain Ocean, which led to re-accretion of YTT to Laurentia and suturing of Slide Mountain Ocean in the late Permian (e.g. Beranek & Mortensen, 2011).

Beranek and Mortensen (2011) referred to late Permian (260-252.5 Ma) collision between YTT and Laurentia as the ‘*Klondike orogeny*,’ although similar versions of this model had been proposed prior to their work by others (e.g. Mortensen, 1992a; Dusel-Bacon *et al.*, 1995; 2002; Nelson *et al.*, 2006; Berman *et al.*, 2007; Colpron *et al.*, 2007; Johnston *et al.*, 2007). Most studies concerning the Paleozoic to early Mesozoic evolution of YTT, SMT and Laurentia conducted since Beranek and Mortensen (2011) have been interpreted within, and supportive of this framework for the Klondike orogeny (e.g. Nelson *et al.*, 2013; Petrie *et al.*, 2015; 2016; Colpron *et al.*, 2015; 2016; Golding *et al.*, 2016a; Staples *et al.*, 2016; Gilotti *et al.*, 2017). Such hypotheses typically cite the following as supporting evidence:

(1) Similarities in lithostratigraphy and detrital zircon populations of pre-Late Devonian metasedimentary basement of YTT and metasedimentary rocks of Laurentia are interpreted as indication that YTT initially formed part of the Laurentian margin prior to rifting (e.g. Colpron *et al.*, 2006a; Piercey & Colpron, 2009).

(2) Occurrences of Mississippian to Permian arc plutonic and volcanic rocks within YTT that are not recorded within Laurentia are interpreted as indications that YTT rifted from Laurentia during the Late Devonian and then evolved independently, remaining allochthonous to Laurentia at least until the end of the Permian (e.g. Mortensen, 1992a; Nelson *et al.*, 2006; 2013). The presence of Mississippian and Permian to Triassic metamorphism in YTT but its absence from Laurentia are also used as evidence for separation until the Triassic (e.g. Berman *et al.*, 2007; Staples *et al.*, 2016).

(3) Outcrops of SMT located along the present-day YTT-Laurentia boundary are interpreted as Slide Mountain ocean floor stratigraphy accreted to YTT and/or Laurentia, marking a suture that formed

following Permian subduction and closure of the Slide Mountain Ocean (e.g. Mortensen, 1992a; Murphy *et al.*, 2006).

(4) Mid-Permian blueschist and eclogite assumed to be metamorphosed slivers of Slide Mountain oceanic crust (e.g. Creaser *et al.*, 1997; 1999; Erdmer *et al.*, 1998), and mid- to late Permian Sulphur Creek plutonic suite and volcanic Klondike schist (collectively referred to as the Klondike assemblage), within YTT (e.g. Mortensen, 1990; Colpron *et al.*, 2006a) have been interpreted as a ‘paired metamorphic belt’ that recorded subduction of Slide Mountain Ocean beneath YTT (e.g. Mortensen, 1992a; Nelson *et al.*, 2006; Beranek & Mortensen, 2011). Beranek and Mortensen (2011) split the Klondike cycle into an early subduction-related phase of arc magmatism, deformation and metamorphism between 260 and 254 Ma and a later phase of crustal-melt derived post-tectonic magmatism between 254 and 252 Ma. These studies bracket the closure of Slide Mountain Ocean and the Klondike orogeny between 260 and 252.5 Ma (Beranek & Mortensen, 2011; Nelson *et al.*, 2013).

(5) The Triassic Jones Lake Formation (Beranek *et al.*, 2010) that overlies parts of Laurentia, SMT and YTT in Yukon and British Columbia has been interpreted as a syn-orogenic sedimentary cover succession initiated in the Early Triassic (e.g. Colpron *et al.*, 2005; 2006; 2007; Beranek *et al.*, 2010; Beranek & Mortensen, 2011; Golding *et al.*, 2016a). Mississippian to Permian detrital zircon populations from these strata have been interpreted as indications of a YTT-derived sediment source, which formed an overlap succession marking the final stages of collision, accretion and related subsidence between YTT and Laurentia (Colpron *et al.*, 2006; 2007; Beranek & Mortensen, 2011).

2.1. Unresolved issues, conflicting datasets and alternative models

Other datasets and models for the tectonic evolution of YTT, SMT and Laurentia disagree, or are hard to reconcile with models of the Klondike orogeny. These are summarized below and are considered in light of our own findings, following presentation of our geochemical and geochronological analyses from the Dunite Peak ophiolite. These include:

(1) Mid-Permian eclogites previously interpreted as metamorphosed slices of SMT oceanic crust have since been identified as mafic intrusions within YTT (Petrie *et al.*, 2016). Furthermore, it has been demonstrated that the YTT metasedimentary rocks which host these intrusions also record mid-Permian eclogite facies metamorphism (Gilotti *et al.*, 2017). As such, deformation, metamorphism and magmatism previously attributed to the Klondike orogeny (e.g. Mortensen, 1990; 1992a; Berman *et al.*, 2007; Beranek & Mortensen 2011; Staples *et al.* 2016; Petrie *et al.*, 2016; Gilotti *et al.*, 2017) are exclusively recorded in YTT, which forms the upper plate in these models. There is no evidence of contemporaneous lower-plate (i.e. Laurentia) deformation or metamorphism to support these models (Berman *et al.*, 2007; Staples *et al.*, 2016).

(2) Existing models do not account for the presence of mid-Permian igneous rocks in SMT with geochemical signatures that require formation in an SSZ setting (e.g. Nelson *et al.*, 1993; Plint & Gordon, 1997; Dusel-Bacon & Cooper, 1999; Fallas *et al.*, 1999; Colpron *et al.*, 2005; 2006b; Dusel-Bacon *et al.*, 2006). These data are incompatible with models which propose that Slide Mountain Ocean subducted beneath YTT during the mid-Permian (e.g. Mortensen, 1992a; Murphy *et al.*, 2006; Nelson *et al.*, 2006; 2013; Johnston *et al.*, 2007; Beranek & Mortensen 2011).

(3) Detrital zircons and conodont fauna do not validate, and in some cases are inconsistent with a model of deposition of Triassic syn-orogenic clastic sediments in a regional-scale basin overlapping YTT, SMT and Laurentia following Permian collision (e.g. Colpron *et al.*, 2007; Beranek *et al.*, 2010; Beranek & Mortensen, 2011). With the exception of three Mississippian zircons, detrital zircon populations of Early Triassic strata on the west Laurentian margin in Yukon (*cf.* Beranek *et al.*, 2010) may be entirely explained by a Laurentian source (Archean, Proterozoic and pre-340 Ma Paleozoic zircons). Middle to Late Triassic strata deposited on Laurentia in Yukon and northern British Columbia contain pre-340 Ma zircons that may be explained by a Laurentian source or by a YTT source, plus Mississippian to Triassic zircons that require either a YTT source (i.e. a Laurentian zircon population plus abundant Mississippian to Permian zircons), or Stikinia/Quesnellia source (i.e. Mississippian, minor Permian and abundant Triassic zircons). In contrast, most Middle Triassic strata overlying SMT in Yukon and northern British Columbia (e.g. Nelson &

Bradford, 1993; Murphy *et al.*, 2002; Colpron *et al.*, 2005) have unimodal/bimodal Permian-Triassic \pm Devonian – Early Mississippian detrital zircon populations (Beranek & Mortensen, 2011). This is suggestive of sediment derived from a late Paleozoic – early Mesozoic arc such as Stikinia/Quesnellia, and is not consistent with sediment derived from YTT \pm Laurentia, which would also contain Pennsylvanian, Devonian to Cambrian, Proterozoic and Archean zircons. In the Finlayson Lake district (Figure 1c), the Late Triassic Bug Island Limestone, which overlies SMT, yielded a detrital zircon population of Laurentian zircons plus five Mississippian zircons that may suggest a YTT source (Beranek, 2009). Conodont fauna from this limestone includes the “exotic” Tethyan species *Norigondolella hallstattensis* (Orchard, 2006) that has been reported from other allochthonous terranes (e.g. Wrangell terrane; Orchard, 1991), but is not recorded from anywhere along the autochthonous Laurentian margin (Orchard, 2006; Beranek, 2009). Additionally, the Bug Island Limestone overlies Middle Triassic clastic sedimentary rocks with unimodal/bimodal zircon populations that are not suggestive of a Laurentian or YTT source (Beranek, 2009; Beranek & Mortensen, 2011). It is therefore unlikely that these Middle to Late Triassic strata that overlie parts of SMT were deposited in the same basin system as coeval strata deposited on Laurentia (Orchard, 2006).

In central to southern British Columbia, Anisian (Middle Triassic) to Rhaetian (Late Triassic) strata overlying Laurentia are interpreted as foreland basin deposits derived from YTT and Laurentia following their collision in the Permian (Golding *et al.*, 2016a). However, detrital zircon populations in these strata can be explained by a Laurentian source with the minor addition of sediment from YTT or Stikinia, to account for the presence of four zircon grains with Mississippian ages and three zircon grains with Permian ages, (Ferri, 2009; Ferri *et al.*, 2010; Golding *et al.*, 2016a). Additionally, Rhaetian clastic strata in central British Columbia analysed by Golding *et al.* (2016b), are dominated by Late Triassic euhedral zircon grains that suggest a volcanic source from Quesnellia. As such, these data indicate that Middle to Late Triassic sedimentary strata in southern and central British Columbia can be explained coherently with sources derived from Laurentia and Stikinia/Quesnellia, with no demand for a YTT sediment source (Golding *et al.*, 2016a, b). As such, detrital zircon data from Triassic strata in Yukon, British Columbia and one sample in Alaska do not indicate that YTT collided and accreted to Laurentia during the Permian.

(4) Paleomagnetic studies from across the Northern Cordillera suggest that between 90-70 Ma and 50 Ma, YTT, SMT and parautochthonous parts of Laurentian were fixed together as they moved northwards to their current position relative to stable North America (see reviews of Gabrielse *et al.*, 2006 and Enkin, 2006). Prior to this, paleomagnetic data from Middle Pennsylvanian – early Permian red cherts from SMT in the Sylvester allochthon (Figure 1a) and at Sliding Mountain, in northern and central British Columbia, suggest that these parts of SMT were deposited $\sim 20^\circ$ south of their current locations with respect to stable North America (Richards *et al.*, 1993). Secondary magnetization suggests that following deposition at equatorial latitudes, these chert units migrated northwards with respect to Laurentia until the Early to Middle Jurassic. Based on the occurrence of an Early Jurassic chemical remagnetization event (Cole *et al.*, 1992) recorded locally within the Cache Creek terrane (Figure 1), and on the intersection of the small circle for the secondary magnetization pole in these chert units with the Middle to Late Jurassic portion of the apparent polar wander path for Laurentia (their Figure 8), Richards *et al.* (1993) favoured an Early to Middle Jurassic timing of obduction and accretion of these SMT units to Laurentia. This contradicts the Permian timing for closure of Slide Mountain Ocean favoured by most authors.

(6) Of most striking contrast to the Klondike orogeny model of Beranek and Mortensen (2011) and others, are the Cordilleran Ribbon Continent models for the Northern American Cordillera (Johnston, 2008; Hildebrand, 2009). These models proposed that parts of the parautochthonous Laurentian margin, such as the Cassiar platform (CA – Figure 1) in Yukon and British Columbia are actually exotic with respect to Laurentia and collided with the intermontane terranes (YTT, Stikinia, Quesnellia) in the Late Triassic to form a composite continental ribbon. Accretion of the ribbon continent to Laurentia is proposed to occur in the Cretaceous (Johnston, 2008; Hildebrand, 2009). This model has received little support from the scientific community (e.g. Monger, 2014; Colpron *et al.*, 2015; Sigloch & Mihalynuk, 2017; Matthews *et al.*, 2017; 2018), partly because the occurrence of a Cretaceous suture between ribbon continent and Laurentia, which should be located inboard of the Cassiar platform, remains cryptic (e.g. Johnston, 2008; Monger, 2014).

3. STUDY AREA: THE DUNITE PEAK OPHIOLITE AND LOCAL GEOLOGY

The Dunite Peak ophiolite (DPO, Figure 1e and 2) forms klippen of mid-Permian mafic-ultramafic rocks (267 ± 10 Ma, de Keijzer *et al.*, 2000) previously assigned to SMT (Figure 2), overlying rocks previously assigned to YTT (Parsons *et al.*, 2017a,b). The location of the DPO study area (Figure 2) with respect to the major terrane boundaries is indicated on Figure 1. The tectonic boundary between YTT and Laurentia (Cassiar terrane, Figure 1), is inferred to lie 5 km east of the study area shown in Figure 2 (Colpron *et al.*, 2016a). This boundary is structurally equivalent to the Middle Triassic to Early Jurassic ductile and post-Jurassic brittle Tummel fault zone (Figure 1i, Colpron *et al.*, 2005) and the post-Late Triassic Inconnu thrust (Murphy *et al.*, 2006). To the west of the study area, the N-S striking d'Abbadie fault system (Figure 2) had an early normal sense of motion and subsequent post-96 Ma right-lateral strike-slip motion with ~4 km dextral displacement that truncated the DPO along its length (de Keijzer *et al.*, 1999; Colpron *et al.*, 2017).

The dominant transposition foliation within the DPO and all underlying units is sub-parallel to compositional layering. Mineral stretching lineations and shear-sense indicators in these units broadly correspond to a NE-SW transport direction, most commonly with a top-SW shear sense. These fabrics are folded by an open synform that plunges gently WSW (Figure 2). The bedrock geology in the Dunite Peak region (Figure 2) may be split into three distinct units, listed from structurally lowest to highest: (1) A basal marble unit; (2) a marine metasedimentary succession; and (3) the Dunite Peak ophiolite. Within each of these, unit subdivisions are identified, as described below. Additional field observations from this area are described by Parsons *et al.*, 2017a, b and de Keijzer *et al.* (1999, 2000).

3.1. Basal marble unit

The structurally lowest unit (Figure 2) comprises coarse grained massively bedded marble, weathered yellow-grey, ≥ 600 m thick, with rare garnet-kyanite bearing metapelitic and garnet-amphibole-epidote bearing meta-igneous layers. This basal marble unit is identified as part of the Snowcap assemblage of YTT based on the occurrence of Mississippian Simpson Range suite orthogneiss within this metasedimentary unit, both north and south of the study area (de Keijzer *et al.*, 2000; Westberg *et al.*, 2009, 2010; Colpron *et al.*, 2016a). Based on its lithology, the basal marble unit probably forms the northern continuation of the

Scurvy Creek succession, a locally defined subdivision of the Snowcap assemblage which crops out 10-30 km south of our study area (Westberg *et al.*, 2009; 2010; Colpron *et al.* 2016a).

3.2. Marine metasedimentary succession

The marine metasedimentary succession has a structural thickness of ~350-500 m (Figure 2) and is visually distinct from the underlying basal marble unit. From bottom to top, this succession divides into four mapped units (Figures 2 and 3a): (1) *MMS1* – Micaceous and carbonaceous quartzite and carbonaceous shale (~100-150 m thick); (2) *MMS2* – white quartzite overlain by interbedded quartzite, marble and subordinate carbonaceous calc-silicate layers (~100 m thick); (3) *MMS3* – a unit of carbonaceous semipelite and shale, which locally contains an upper portion of thinly interbedded carbonaceous shale/semipelite and subordinate chert, quartzite (silt/sandstone) and metavolcanics (150-250 m thick); at one outcrop, pillow basalt was also observed within this unit; and (4) *MMS4* – dark grey, micritic, mylonitized marble (200-250 m thick) with locally less deformed and fossiliferous zones containing deformed bryozoa and unidentified shelly fauna.

Mylonitic foliation within the marine metasedimentary succession increases in deformation intensity up-section towards the base of the DPO crustal section. A metamorphic assemblage of biotite \pm garnet \pm staurolite \pm chlorite suggests that this unit is of a lower metamorphic grade than the basal marble unit. Based on its lithology and structural relationship with the basal marble unit we speculate that the marine metasedimentary succession may correlate with either the Nasina assemblage or Swift River Group of the Finlayson assemblage (e.g. Colpron *et al.*, 2006a; Nelson *et al.*, 2006).

3.3. The Dunite Peak ophiolite (DPO)

The DPO has a variable structural thickness of ~450 m to >1650 m, and comprises a crustal section of mafic to intermediate volcanic/volcaniclastic and plutonic rocks, structurally overlain by ultramafic rocks (Figures 2 and 3).

Crustal Section (DPc)

The DPO crustal section (*DPc*, Figure 2) is an internally deformed thrust stack of metamorphosed basaltic to andesitic volcanics and volcaniclastics, gabbro and leucogabbro with a variable thickness of ~300-650 m (Figures 2 and 3). The degree of metamorphism and deformation in these rocks is such that it is often not

possible to distinguish between volcanic, volcanoclastic and hypabyssal lithologies. Henceforth, we use the term 'greenstone' to collectively refer to the metamorphosed products of these rock types. Generally, the lithologies of this unit (Figure 4) transition from a lower portion of fine to medium grained (≤ 1 mm) greenstone to an upper coarser grained portion of interlayered greenstone, gabbro and leucogabbro.

The base of the DPO crustal section is dominated by light green, very fine grained, homogeneous and locally fissile greenstone with rare pelitic and silicic horizons and sheared pillows (Figure 4a-c). These rocks probably represent volcanic and volcanoclastic successions erupted/deposited in a subaqueous environment with intermittent chert and argillite deposition. Up-section, the DPO crustal section is dominated by gabbro and coarser grained pyroxene- \pm plagioclase-phyric greenstone that probably represent a mix of plutonic and vent-proximal volcanic and hypabyssal successions (Figure 4d-e). In the upper portion of the crustal section, pelitic and silicic horizons are not observed, and gabbro and leucogabbro commonly intrude greenstone (Figure 4e-f). Variability in grain size and in relative proportions of leucocratic to melanocratic minerals within the gabbro and leucogabbro define compositional layering sub-parallel to foliation with locally undulating and discordant boundaries corresponding to original intrusive relationships. The top of the crustal section consists of medium to coarse grained (~ 0.5 -2 mm) cumulate to adcumulate gabbro, leucogabbro and plagiogranite and subordinate fine grained greenstone layers (Figure 4f). Leucogabbro contains rare rafts of greenstone.

The DPO crustal section is pervasively sheared with a mylonitic fabric at its lower and upper contacts. Thrust imbrication of this unit incorporates thrust-bounded slivers of the marine metasedimentary succession (MMS3, Figure 2). A peak metamorphic mineral assemblage of hornblende-actinolite + epidote-clinozoisite + albite-oligoclase is indicative of upper greenschist to lower amphibolite facies conditions. Peak metamorphic conditions do not appear to vary between vertical structural positions or between metavolcanic/volcanoclastic units and metaplutonic units. As such, the observed metamorphism of the DPO probably corresponds to burial and heating during or after emplacement, rather than metasomatism during ophiolite formation, which would display increasing metamorphic grade from supracrustal to plutonic sections of an ophiolite.

Ultramafic Section (DPu)

The ultramafic section of the DPO is the structurally highest unit (*DPu*, Figures 2 and 3) and forms isolated klippen emplaced onto the DPO crustal section (*DPc*) with variable thicknesses of ~150 m to >1000 m (Figures 2-3). The lowermost ~5-50 m of these klippen (*DPu1*, Figure 2) are ubiquitously defined by sheared, locally cataclastic blue-green and dark-blue-black ‘fish-scale’ serpentinite (Figure 3b). This transitions up-section into orange-weathered, variably serpentinized harzburgite and dunite with subordinate lherzolite (*DPu2*, Figure 2). Pyroxene-rich layers define compositional layering within these rocks, which vary in orientation across the klippen. Planar intrusions of pyroxenite and gabbro cross-cut these ultramafic rocks (*DPu3*, Figures 2 and 3b). Dunites contain aggregates of undeformed olivine and serpentine-psuedomorphs of olivine with interlocking, adcumulate textures and no interstitial material between grains. Harzburgites contain orthopyroxene phenocrysts with oikocrysts of olivine and clinopyroxene, plus chromite with orthopyroxene overgrowths that may be indicative of exsolution cumulate residuum. The basal serpentinite of the DPO ultramafic section (*DPu1*) displays S-C fabrics with C-planes parallel to mylonitic foliation in underlying DPO crustal section. S-planes show no consistent transport direction. Above this, thrust faulting and chaotic folding decrease in intensity up-section until they are absent from the orange-weathered upper portion of planar-stratified ultramafic layers (*DPu2*).

4. U-Pb ZIRCON GEOCHRONOLOGY

Zircon U-Pb isotopic analysis was conducted for geochronology on sample 16RAY-AP074A1; a coarse grained gabbro intruded into greenstone from the top of the DPO crustal section (Figure 2). This gabbro does not cross-cut the deformation fabric in the greenstone. Analyses were conducted by secondary ion microprobe spectrometry (SIMS) at the U.S. Geological Survey-Stanford University SHRIMP-RG (sensitive high resolution ion microprobe-reverse geometry) facility. Analytical procedures are described in detail in Supplementary Materials 01. The full U-Pb isotopic dataset is presented in Supplementary Materials 02.

Sample 16RAY-AP074A1 yielded euhedral to subhedral zircon with oscillatory zoning and some thin cathodoluminescence (CL) dark, high-U rims that may reflect resorption (Figure 5a). Spot analyses (Figure 5a) conducted on 12 zircon grains produce a simple cluster of grain ages overlapping concordia and, excluding the oldest analysis, define a weighted mean $^{206}\text{Pb}/^{238}\text{U}$ age of 265 ± 4 Ma (MSWD = 0.9; Figure

5b). The oldest analysis (283 ± 4 Ma) was obtained from a euhedral, CL-bright, low-U (50 ppm) grain core domain (spot 4.1, Figure 5a) and inclusion of this grain yields a mean age of 268 ± 6 Ma (MSWD = 2.7). Whilst analytical scatter cannot be ruled out, textural evidence suggests that the core domain represents a xenocryst that records an earlier magmatic history. Chondrite-normalized trace element signatures are depleted in LREEs relative to HREEs and have little variation between each grain (Figure 5c). Together, the trace element signatures, grain morphology and spread of individual grain ages suggest that the calculated mean age reflects the timing of crystallization of the magmatic protolith. Ti-in-zircon thermometry (Ferry & Watson, 2007) yields a mean zircon crystallization temperature of 761 ± 21 °C (1σ error).

5. GEOCHEMISTRY

The degree of metamorphism and deformation recorded by the DPO makes it difficult to identify and distinguish between specific igneous protoliths using field observations and optical microscopy alone. We utilize whole-rock major and trace element and Sm-Nd isotopic analyses to provide additional constraints on protoliths and igneous petrogeneses of different rock types in the DPO. Whole-rock geochemical analyses of 52 samples were conducted by Activation Laboratories Ltd. (Ancaster, ON). Sm-Nd isotopic analysis of 7 samples was conducted at Carleton University (Ottawa, ON). Analytical procedures for both analyses are described in Supplementary Materials 01.

5.1. Immobile element fingerprinting

For interpretation of the whole-rock element analysis, only immobile rare earth elements (REEs) and high field strength elements (HFSEs) are considered, in order to minimize the effects of element mobility during metamorphism (e.g. Pearce, 1996; 2014). REE-HSFE profiles (Figure 6) and normalized element concentrations and ratios (Table 1) are given relative to N-MORB (Sun & McDonough, 1989, plus V and Sc from Klein, 2004) for Groups 1-4, defined below and relative to primitive mantle (Sun & McDonough, 1989, plus V and Sc from McDonough & Frey, 1989) for Group 5, defined below. Immobile element ratios Nb/Y and Zr/Ti provide proxies for $\text{Na}_2\text{O} + \text{K}_2\text{O}$ (total alkalinity) and SiO_2 , respectively (Cann, 1970; Pearce, 1996) (Figure 7a). Fractionation of immobile elements Y, La and Nb provides a means to classify crustal samples in terms of magmatic setting, due to the variable sensitivity of these elements to degree of partial

melting/fractionation, composition of melt source and subduction zone interaction (Figure 7b) (Cabanis & Lecolle 1989). Relative concentrations of Th, Nb, and Yb, provide a means to distinguish suprasubduction zone (SSZ) settings from intra-plate and mid-ocean spreading ridge settings (Figure 7c) (Pearce, 2008, 2014). Th and Nb behave similarly in the mantle ($\text{Th/Nb} \approx 1$), except during subduction where Nb is retained in the subducting slab, whilst Th is released from the subducting slab into the mantle wedge. This results in high positive Th/Nb ratios in mantle wedge-derived magmas (Pearce, 2008). The concentration of Yb, relative to Th and Nb provides an indication of degree of fractionation, which may be used to distinguish intra-oceanic arc from continental arc settings and mid-ocean ridge from intra-plate settings (Pearce, 2008; 2014).

From the 52 samples analyzed, five geochemically distinguishable groups are defined. Groups 1 to 3 contain mafic to intermediate samples from the DPO that are distinguished from each other on geochemical bases, irrespective of lithology, following the identification of three distinct geochemical signatures. Group 4 contains a single sample of pillow basalt from the marine metasedimentary succession (MMS3). Group 5 contains ultramafic samples from the DPO. Locations of samples are given in Figure 2 with group-specific symbology. Seven fine-grained greenstone samples from the DPO were selected for Sm-Nd isotopic analysis prior to distinction of Groups 1 to 3. Of these seven samples, four derive from Group 1 and three derive from Group 3. The results of Sm-Nd isotopic analyses are reported alongside the whole-rock analyses of these groups.

Group 1 (DPO mafic to intermediate rocks)

Group 1 ($n = 18$) displays LREE enriched spectra and large Th/Nb anomalies (Figure 6a), and may be divided into two subgroups based on the relative concentrations of Ti, V and Sc (Figure 6a). Group 1a has less enrichment ($[\text{La/Yb}]_N = 2.87$, $\text{La}_N = 1.08$, $[\text{Th/Nb}]_N = 14.67$) than Group 1b ($[\text{La/Yb}]_N = 4.68$, $\text{La}_N = 4.21$, $[\text{Th/Nb}]_N = 27.95$). Group 1a displays minor negative and a single strong positive Ti anomaly. V and Sc are enriched relative to other HREEs and Ti. These samples display minor negative anomalies in Zr-Hf (Figure 6a). In contrast, Group 1b displays strong negative Ti, V and Sc anomalies, but no Zr-Hf anomalies (Figure 6a). Small positive Eu anomalies are common in both subgroups. Sm-Nd isotopic analysis of four

samples from Group 1 yielded $\mathcal{E}_{Nd(t=265)}$ values of +7.2, +7.4, +7.5 (Group 1a) and +7.4 (Group 1b) (Table 1).

Group 2 (DPO mafic to intermediate rocks)

Group 2 ($n = 11$, Figure 6b) displays moderately LREE-enriched to flat spectra ($[La/Yb]_N = 2.91$). Element concentrations are depleted relative to N-MORB by up to a factor of 10 ($La_N = 0.85$, $Yb_N = 0.32$). Group 2 samples have large Th/Nb ratios ($[Th/Nb]_N = 17.43$), negative Ti anomalies and strong positive V and Sc anomalies relative to HREEs and Ti (Table 1). Negative Zr-Hf anomalies and positive Eu anomalies are sometimes displayed (Figure 6b).

Group 3 (DPO mafic to intermediate rocks)

Group 3 ($n = 6$, Figure 6b) displays flat spectra ($[La/Yb]_N = 1.41$) with N-MORB-comparable concentrations ($La_N = 1.49$, $Yb_N = 1.07$). All samples have positive Th/Nb ratios ($[Th/Nb]_N = 5.29$) and negligible to small positive V anomalies, negative Sc anomalies, but no significant Ti or Eu anomalies. Three samples from Group 3 yielded $\mathcal{E}_{Nd(t=265)}$ values of +8.3, +8.1 and +9.0 (Table 1).

Group 4 (pillow basalt)

Group 4 ($n = 1$, Figure 6c) has an LREE-enriched spectrum ($[La/Yb]_N = 2.14$) with N-MORB-comparable concentrations of HREEs ($La_N = 1.42$, $Yb_N = 0.66$). Unlike Groups 1-3, Group 4 has no Nb anomaly ($[Th/Nb]_N = 1.55$), nor does it have Ti, V, Sc or Eu anomalies (Table 1).

Group 5 (DPO ultramafic rocks)

Group 5 ($n = 16$, Figure 6d) comprises samples from the DPO ultramafic section (*DPu*). CIPW normative major element concentrations of Group 5 samples mostly plot within the harzburgite (6 samples) and dunite (6 samples) fields. A minority plot within lherzolite (3 samples) and pyroxenite (1 sample) fields (Figure 7d). Two reference compositions for depleted-MORB mantle (DMM – Salters & Stracke, 2004; Workman & Hart 2005) are also included on the REE-HFSE diagram (Figure 6d). Group 5 is depleted in HREEs relative to primitive mantle and DMM ($Yb_N = 0.21$). LREEs are enriched relative to HREEs and DMM (La_N

= 0.50, $[La/Yb]_N = 2.37$). Several samples have positive Th anomalies equal to, or greater than primitive values ($Th_N = 1.06$), and most have Nb concentrations below the analytical detection limit. One sample had detectable amounts of both Th and Nb, producing $[Th/Nb]_N = 14.26$. Positive V and Sc and Zr anomalies are common.

5.2. Interpretation of geochemistry results

Group 1 comprises greenstone and gabbro from the DPO crustal section (Figure 6a). Differences between Groups 1a and 1b probably reflect crystal fractionation processes. Group 1a plots within subalkaline basaltic to basaltic andesite island arc tholeiite (IAT) fields and probably represents plutonic/hypabyssal IATs (Figure 7a-b). These samples have positive V, Eu, and Sc anomalies, plus one positive Ti anomaly, and negative Zr-Hf anomalies. These are generally attributed to crystallization and retention of magnetite/rutile (Ti enrichment) and clinopyroxene (Sc enrichment) and extraction of an intermediate-acid melt (Zr-Hf depletion) (e.g. Pearce, 1996). Positive V anomalies are generally attributed to hydrous mantle melting (e.g. Pearce, 2014). Positive Eu anomalies are most easily explained by the presence of cumulate plagioclase (e.g. Rollinson, 1993). Positive Th/Nb ratios and negative Nb anomalies suggest a SSZ setting (Figure 7c).

Group 1b plots within basaltic-andesite to andesite IAT–calc-alkaline (CA) fields (Figure 7a-b) and represents a more fractionated component of IAT to CA hypabyssal magmatism or volcanism. This is suggested by negative Ti anomalies and the absence of Zr-Hf anomalies; Ti is depleted in moderately evolved magmas due to early fractionation of Ti-bearing phases in basaltic magmas, whereas Zr and Hf remain incompatible during fractionation of intermediate melts. Negative Sc anomalies can be attributed to early clinopyroxene fractionation in basaltic magmas. Negative V anomalies may be attributed to increased compatibility of V during crystal fractionation of intermediate melts (e.g. Pearce, 1996). Positive Th/Nb ratios and negative Nb anomalies suggest a SSZ setting (Figure 7c). ϵ_{Nd} values from Groups 1a and 1b ranging between +7.2 and +7.5, indicate that these magmas did not interact with continental crust (e.g. Rollinson, 1993).

Group 2 comprises layered gabbro, leucogabbro and subordinate greenstone from the DPO crustal section (Figure 6b) with subalkaline basaltic to basaltic andesite compositions (Figure 7a). These data form an array

from the intersection between IAT-CA and CA fields to the intersection between IAT, N-MORB and back-arc basin basalt (BABB) fields, mostly plotting in the IAT field (Figure 7b). Based on the same interpretations as provided for Group 1a (*see above*), the depleted nature of Group 2 including Zr-Hf negative anomalies and V-Sc positive anomalies suggests that these rocks represent crustal cumulates derived from hydrous mantle melting. Variations in Ti and V most likely reflect variable proportions of cumulate phase (Ti depleted) versus melt phase (Ti enriched) \pm later addition of Ti-bearing fluids, as suggested by the presence of titanite veins in some samples. Positive Th/Nb ratios and negative Nb anomalies suggest a SSZ setting (Figure 7c).

Group 3 comprises gabbro intrusions from the DPO ultramafic section and greenstone from the DPO crustal section (Figure 6b) with subalkaline basaltic N-MORB-comparable compositions (Figure 7a-b) plus Nb and V anomalies suggesting subduction zone interaction (Figure 7c) and hydrous mantle melting (e.g. Pearce, 1996; 2014). Minor negative Sc anomalies probably reflect earlier crystallization of clinopyroxene (e.g. Pearce, 1996). Group 3 is interpreted as primary BABB melts derived directly from depleted mantle, with little or no subsequent crystal fraction or melt extraction. Positive Th/Nb ratios and negative Nb anomalies suggest a SSZ setting (Figure 7c). ϵ_{Nd} values from Group 3 ranging between +8.8 and +9.0, indicate that it has not interacted with continental crust (ϵ_{Nd} of depleted mantle = 9.0-9.6, Kimura *et al.*, 2017).

Group 4 is a pillow basalt sample from the marine metasedimentary succession (Figure 6c), and has a geochemical signature comparable to subalkaline E-MORB (Figure 7a-c). The stratigraphic association of Group 4 with the marine metasedimentary succession and absence of E-MORB signatures from the DPO (one Group 1a sample excepted) suggest that Group 4 does not derive from the same SSZ setting as Groups 1-3.

Group 5 comprises ultramafic rocks from the DPO (Figure 6d) that displays lithological, petrographic (see Section 3.3) and geochemical characteristics typical of lower crustal or mantle cumulates, rather than mantle tectonites. It is dominated by dunite and harzburgite with cumulate and adcumulate textures. Enrichment in LREEs relative to HREEs and large V/Ti ratios suggest that Group 5 derived from partial melting of the mantle under hydrous conditions. Positive Sc anomalies probably reflect the presence of cumulate

clinopyroxene. Positive Zr anomalies may correspond to enrichment from slab-derived fluids (e.g. Bizimis *et al.*, 1999) or recycling of lower crustal material during crustal foundering (e.g. Arndt & Goldstein, 1989). Strong depletion in Nb (all but one Group 5 sample have Nb concentrations below the detection limit), and enrichment in Th and the presence of BABB intrusions (Group 3) within these rocks suggests that the DPO ultramafic section formed in the same SSZ setting as Groups 1-3.

6. PETROGENESIS OF THE DUNITE PEAK OPHIOLITE

Large Th/Nb ratios, large positive ϵ_{Nd} values, enriched concentrations of LREEs and N-MORB-comparable concentrations of HREEs indicate that the DPO is an SSZ ophiolite (Figure 7b-c) comprising a dismembered crustal section and lower crustal/lithospheric mantle cumulates of an intra-oceanic arc system. U-Pb zircon geochronometry from a Group 2 IAT gabbro (this study, Figures 2 and 5) and a leucocratic granitic dike (de Keijzer *et al.*, 2000, Figure 2) within the DPO crustal section yielded respective ages of 265 ± 4 Ma and 267 ± 10 Ma. The ages and geochemical signatures of these rocks suggest that constructional volcanism was occurring along an intra-oceanic arc that resided somewhere within the ocean separating YTT and Laurentia during the mid-Permian (currently modelled as the Slide Mountain Ocean). The single zircon xenocryst age (283 ± 4 Ma) from sample 16RAY-AP074A1 (this study), may derive from the Group 1 IAT greenstone into which it intrudes (e.g. Figure 4e-f), corresponding to the earliest record of magmatism along this intra-oceanic arc. Comparison of volcanic glass and whole rock REE-HFSE signatures of basalt, basaltic andesite and andesite samples collected from four active intra-oceanic arc settings in the SW Pacific Ocean (Figure 8) with geochemical signatures from the Dunite Peak ophiolite supports our interpretation that the Dunite Peak ophiolite derived from an intra-oceanic arc system (Figure 8b, e) in which arc (IAT/CA) and subordinate back-arc (BABB) magmatic assemblages were generated co-spatially (Figure 8c, f).

6.1. Correlative SSZ ophiolites in the Northern Cordillera

The DPO is comparable to other mid-Permian ophiolites currently assigned to SMT that comprise sections of oceanic crust and lithospheric mantle with mafic to intermediate SSZ geochemical signatures (e.g. Mortensen, 1990; Nelson & Bradford, 1993; Dusel-Bacon *et al.*, 2006; Petrie *et al.*, 2015). These comparable sections are as follows:

In Division II of the Sylvester allochthon, north British Columbia (Figure 1a), the Quartzrock Creek gabbro, Cassiar block, Zus Mountain block and Blue Mountain block form ophiolitic sections of coarse grained cumulate gabbro and leucogabbro, layered clinopyroxene and dunite and tectonized harzburgite (Gabrielse *et al.*, 1993; Nelson, 1993; Nelson & Bradford, 1993). U-Pb zircon geochronology from a layered leucogabbro in the Zus Mountain block yielded an age of $268.6 \pm 6.8/-3.4$ Ma (Figure 1a) (Gabrielse *et al.*, 1993). Geochemical signatures from Division II basalts (Nelson, 1993) are mostly N-MORB; however a minority of these samples have arc signatures (IAT or CA) requiring an SSZ setting.

In south-central Yukon, the St Cyr klippe and Tower Peak assemblage (Figure 1d) comprise harzburgite, gabbro, leucogabbro and basaltic to andesitic metavolcanic rocks currently assigned to SMT (Fallas *et al.*, 1998; 1999; Petrie *et al.*, 2015). Andesitic greenschists from the Tower Peak assemblage have IAT to CA geochemical signatures (Fallas *et al.*, 1999) indicative of a SSZ setting. In the Finlayson Lake district (Figure 1c) most occurrences of SMT have N-MORB, E-MORB and OIB geochemical signatures. However, localized occurrences of SMT greenstone, gabbro and leucogabbro have signatures ranging between IAT/CA, BABB and N-MORB (Plint & Gordon, 1997; Murphy *et al.*, 2006; Piercey *et al.*, 2012) suggestive of a SSZ setting. Locally, in the Finlayson Lake district (Figure 1c), gabbro and leucogabbro are commonly observed intruding greenstone (Plint & Gordon, 1997), as is observed in the DPO. U-Pb zircon geochronology of a leucogabbro, and of a plagiogranite within a serpentized shear zone (Figure 1c-d), respectively yielded crystallization ages of 273.4 ± 1.4 Ma (Murphy *et al.*, 2006) and 274.3 ± 0.5 Ma (Mortensen, 1992b).

In the Glenlyon region, central Yukon, the Tummel fault zone (Figure 1i) forms the boundary between YTT and Laurentia, comprising fault slices of SMT serpentized harzburgite mantle tectonite, gabbro, greenstone and associated marine sedimentary rocks (Colpron *et al.*, 2005, 2006b). Greenstones have basaltic to andesitic compositions and geochemical signatures that mostly range between N-MORB and IAT (Colpron *et al.*, 2005, 2006b), suggesting an SSZ origin. To the northwest, the Ragged Lake klippe (Figure 1j) comprises serpentinite and gabbro, structurally overlying Laurentia with an IAT/CA geochemical signature (Colpron *et al.*, 2005, 2006b). U-Pb zircon geochronology from an IAT andesitic greenstone in the

Tummel fault zone and from the IAT/CA gabbro in the Ragged Lake klippe respectively yielded crystallization ages of 267.8 ± 1.5 Ma and 260.3 ± 0.8 Ma (Figure 1, Colpron *et al.*, 2005, 2006b).

In west-central Yukon and east-central Alaska, ophiolitic klippen of SMT and the Seventymile terrane (Alaskan correlative of SMT) structurally overlie YTT, comprising pyroxene-phyric greenstone, cumulate gabbro, harzburgite, dunite and subordinate clinopyroxenite (Figure 1o, Foster & Keith, 1974; Foster *et al.*, 1994; Mortensen, 1990; Dusel-Bacon *et al.*, 2006). Notable ophiolite occurrences include Clinton Creek (Mortensen, 1990; Dusel-Bacon *et al.*, 2006), Mount Sorensen, Salcha River and American Creek (Foster *et al.*, 1994; Dusel-Bacon *et al.*, 2006). Geochemical signatures of greenstones in the Eagle quadrangle (Alaska) and Clinton Creek/Dawson area (Yukon) (Figure 1o) range between N-MORB, BABB and CA (Dusel-Bacon *et al.*, 2006), suggestive of a SSZ setting. Metaharzburgite in the Eagle quadrangle has a similar Nb depletion and Th enrichment to our Group 5 DPO samples that is suggestive of a SSZ setting (Dusel-Bacon *et al.*, 2013). Most notably, the Wolf Mountain klippe is dominated by greenstone with basaltic to andesitic and IAT to CA geochemical signatures (Dusel-Bacon & Cooper, 1999; Dusel-Bacon *et al.*, 2006) that closely resemble IAT/CA greenstone from the DPO.

7. THE DUNITE PEAK INTRA-OCEANIC ARC

As outlined above, mid-Permian SSZ ophiolites with mean crystallization ages of ~275-260 Ma (including the DPO), are distributed along the structural boundary between YTT and Laurentia over a distance of ~1000 km between northern British Columbia, Yukon and eastern Alaska (Figure 1). Based on their similar lithological, structural, geochemical and geochronological characteristics, we propose that collectively, they represent tectonic slivers of a regionally extensive intra-oceanic extensional arc system that was active within the Slide Mountain Ocean from 275 and 260 Ma. If our oldest zircon dated from IAT gabbro sample 16RAY-AP074A1 (283 ± 4 Ma) was inherited from the greenstone layer also of IAT composition (sample 16RAY-AP074A2, Table 1), into which it intrudes, then magmatism along this intra-oceanic arc occurred as early as ~280 Ma. This is the first recognition of this arc system, which we define here as the *Dunite Peak intra-oceanic arc*.

The DPO and correlative ophiolitic sections at the Tummel fault zone and Ragged Lake, St Cyr and Wolf Mountain klippen (Figure 1) are dominated by basaltic to andesitic arc-magmatic rocks (IAT/CA), which we interpret as constructional volcanic centers along the Dunite Peak intra-oceanic arc. Correlative ophiolitic sections in the Sylvester allochthon (Figure 1a) and Finlayson Lake district (Figure 1c) have been interpreted as remnants of a fossil transform fault system (Nelson & Bradford, 1993; Murphy *et al.*, 2006; Piercy *et al.*, 2012) or ocean core complexes and syn-volcanic extensional faults (Ryan *et al.*, 2015), and yield geochemical signatures indicative of extensional magmatism in an SSZ setting (BABB, N-MORB \pm E-MORB). We interpret these sections as extensional magmatic zones along the Dunite Peak intra-oceanic arc.

The distribution of constructive volcanic centers (e.g. DPO, Wolf Mountain klippe) and extensional magmatic zones (e.g. Zus Mountain block, Sylvester allochthon) suggests that the Dunite Peak intra-oceanic arc may represent a *disorganized extensional intra-oceanic arc* (e.g. Weissel *et al.*, 1981; Tamaki, 1985; Wysoczanski *et al.*, 2010). These systems are characterized by constructional volcanic centers surrounded by localized zones of disorganized extensional faulting and associated magmatism. Extensional magmatism, typically considered indicative of back-arc spreading (BABB) may occur along strike, adjacent to, and contemporaneous with constructive arc-related magmatism (IAT/CA). Modern examples of disorganized extensional intra-oceanic arcs include the Kermadec arc – Havre trough system (Wysoczanski *et al.*, 2006; 2010; Smith *et al.*, 2009), and the Lau basin (Keller *et al.*, 2008; Sleeper & Martinez, 2014; Sleeper *et al.*, 2016) in the SW Pacific Ocean (Figure 8) and the Calabrian arc in the Mediterranean Sea (Florio *et al.*, 2011). In the geological record, comparable disorganized extensional intra-oceanic arc systems have been inferred for the ancient settings of the Permian Nahlin ophiolite of the Cache Creek terrane in northern British Columbia (McGoldrick *et al.*, 2017) and the Middle Ordovician Annieopsquotch Accretionary Tract of the Newfoundland Appalachians (Zagorevski *et al.*, 2015). The development of the Dunite Peak intra-oceanic arc as a disorganized extensional intra-oceanic arc provides a plausible explanation for the relatively small volume of identifiable remnants of this arc and its elusiveness in the geological record.

8. INTEGRATION WITH EXISTING DATASETS: A NEW HYPOTHESIS FOR THE LATE PALEOZOIC – EARLY MESOZOIC TECTONIC EVOLUTION OF THE NORTHERN CORDILLERA

Slide Mountain Ocean could not have formed the lower plate of a westward-dipping subduction zone beneath YTT (e.g. Mortensen, 1992a; Nelson *et al.*, 2006; Beranek and Mortensen, 2011), at the same time that it generated SSZ ophiolites with upper-plate intra-oceanic arc geochemical compositions (as required by geochemical and geochronological constraints). This would require a more complicated double subduction zone model that would still fail to adequately explain the variable duration and timing of YTT eclogitization, SSZ ophiolite formation, Klondike cycle magmatic rocks and mid-Permian to Middle Triassic exhumation of YTT. We propose an alternative model: structural juxtaposition of mid-Permian SSZ ophiolites and mid-Permian YTT eclogites along the eastern margin of YTT (Figure 1) (e.g. Fallas *et al.*, 1998; Petrie *et al.*, 2015, 2016; Gilotti *et al.*, 2017) by *eastward* subduction and collision of YTT (*lower plate*) beneath the Dunite Peak intra-oceanic arc (*upper plate*) (Figure 9). In the following sections, we present a new hypothesis for the Klondike orogeny (Figure 9) in the context of our analyses of the Dunite Peak ophiolite, combined with existing datasets from across the Northern Cordillera. This includes datasets that were previously inconsistent or hard to reconcile with previous models (*see Section 2.1*). Our proposed model is supported by an extensive geochronology dataset (total of 110 published ages), displayed in Figure 10 (see Supplementary Materials 05 for details), to constrain the timing of specific events. Note that in our model, use of the term ‘*Klondike orogen*’ refers to the accreted mass (i.e. composite terrane) of YTT and the Dunite Peak intra-oceanic arc.

8.1. Mid- to late Permian arc-continent collision: the Klondike orogeny

~280-260 Ma: Dunite Peak intra-oceanic arc magmatism and subduction and collision of YTT continental crust

Subduction related magmatism within the Dunite Peak intra-oceanic arc (Figure 1) is bracketed between ~280 and 260 Ma (Figures 9a & 10, this study; Mortensen, 1992b; Gabrielse *et al.*, 1993; de Keijzer *et al.*, 2000; Colpron *et al.*, 2005; 2006b; Murphy *et al.*, 2006). Along the length of this intra-oceanic arc,

lithological and geochemical variations between ophiolites (see Sections 6.1 and 7) probably reflect development of constructive volcanic centers and localized zones of upper-plate extension and associated magmatism, representative of a disorganized extensional intra-oceanic arc such as the present day Kermadec arc – Havre trough system (e.g. Wysoczanski *et al.*, 2010). It is expected that most of the lower plate oceanic lithosphere subducted into the mantle during that period, although some lower plate material may have accreted to the Dunite Peak intra-oceanic arc (blue accretionary prism, Figure 9a). Early Permian and older occurrences of SMT that contain chert, argillite and pillow basalt with mid-ocean ridge and/or within-plate geochemical signatures such as parts of the Campbell Range basalts in the Finlayson Lake district (Figure 1c, Murphy *et al.*, 2006; Piercy *et al.*, 2012) may represent accreted remnants of this oceanic lower plate.

Subduction and collision of YTT continental crust beneath the Dunite Peak intra-oceanic arc began as early as ~275 Ma (Figure 10, Gilotti *et al.*, 2017) and continued, coeval with magmatism in the Dunite Peak intra-oceanic arc to ~260 Ma (Figures 1e, h, i, g & 10, Creaser *et al.*, 1997; Fallas *et al.*, 1998; Godwin-Bell, 1998; Petrie *et al.*, 2016; Gilotti *et al.*, 2017). Many of the recorded eclogite occurrence from YTT are described as eclogite pods hosted within amphibolite, greenschist or blueschist facies rocks (e.g. Erdmer *et al.*, 1998; Fallas *et al.*, 1998; Petrie *et al.*, 2015). Where blueschist is preserved, such as in the Faro, Ross River and St Cyr regions (Figure 1d, g-h), muscovite cooling ages of ~263 to 235 Ma (Erdmer *et al.*, 1998; Fallas *et al.*, 1998) suggest that these rocks may represent lower plate material from an accretionary complex that formed above the subduction zone between YTT and the Dunite Peak intra-oceanic arc (e.g. blue shaded accretionary complex, Figure 9a). However, most exposures of SMT and/or the Dunite Peak intra-oceanic are structurally interleaved with slices of YTT and/or Laurentia (e.g. Mortensen, 1990; Fallas *et al.*, 1998; Murphy *et al.*, 2006; Petrie *et al.*, 2015) suggesting that the original accretionary complex and subduction interface between YTT and the Dunite Peak intra-oceanic arc has been overprinted or structurally displaced from its original configuration. The arrangement of ultramafic over mafic rocks in the DPO and the apparent absence of a metamorphic discontinuity between the DPO and the underlying YTT also suggest that emplacement structures relating to the original subduction zone and accretionary complex between YTT and the Dunite Peak intra-oceanic arc have been structurally overprinted and/or displaced. This probably

occurred during subsequent regional metamorphism and deformation record in YTT during the latest Triassic to Early Jurassic and Late Jurassic to Early Cretaceous (e.g. Staples *et al.*, 2016).

Amphibolite facies metamorphism of YTT metasedimentary units (Snowcap assemblage) in Canada recorded at ~260 Ma (Berman *et al.*, 2007), 259.3 ± 3.4 Ma (Villeneuve *et al.*, 2003) and 263.6 ± 3.4 Ma (Staples, 2014) probably relates to crustal thickening during the final stages of subduction and collision of YTT (Figures 1 & 10). Subduction and eclogitization of YTT and associated magmatism in the Dunite Peak intra-oceanic arc ceased sometime between 265 and 260 Ma (Figure 10). Based on the ages listed here, we define the earliest record of subduction and collision of YTT (~275 Ma) as the start of the Klondike orogeny (Figure 10).

The coeval generation of SSZ ophiolites in the Dunite Peak intra-oceanic arc and eclogite facies metamorphism of YTT suggests collision was diachronous. This may imply that the subducting margin of YTT had an irregular shape with promontories and re-entrants and/or that collision of YTT with respect to the intra-oceanic arc was oblique (e.g. Cawood & Suhr, 1992). Similarly, we have no constraint on the length of the Dunite Peak intra-oceanic arc, and so it is possible that YTT collided only with a portion of the arc and that adjacent to the subducting YTT, normal oceanic subduction and associated intra-oceanic arc magmatism was maintained. Present-day collision and subduction of the Australian continent adjacent to subduction of oceanic lithosphere beneath the Solomon – New Hebrides intra-oceanic arc is a modern example of this process (e.g. Hall, 2002). Because of these potential and likely complexities and the lack of further constraints, we make no attempt at estimating the width of oceanic crust subducted beneath the Dunite Peak intra-oceanic arc.

265-252 Ma: Slab break-off, subduction polarity reversal, orogenic collapse and associated magmatism

The period between 265 and 260 Ma (Figure 10) marks; (1) the latest occurrence of eclogite facies metamorphism of YTT, and magmatism in the Dunite Peak intra-oceanic arc (*see above*); (2) the earliest record of exhumation and cooling of YTT blueschist and eclogite (Wanless, *et al.*, 1978; Erdmer & Armstrong, 1988; Erdmer *et al.*, 1998; Fallas *et al.*, 1998); (3) the emplacement of orogenic peridotite within YTT (Canil *et al.*, 2003; Johnston *et al.*, 2007); and (4) the beginning of the Klondike magmatic cycle within

YTT (e.g. Colpron *et al.*, 2006a; Beranek & Mortensen, 2011). We interpret the temporal overlap of these events between 265 and 260 Ma (Figure 10) as a record of cessation of subduction of YTT continental lithosphere accompanied or soon followed by orogenic collapse and associated magmatism (Figure 9b).

The Buffalo Pitts peridotite (Figure 1m) has been interpreted as megaboudin of orogenic mantle peridotite emplaced into metasedimentary rocks of YTT during lithospheric extension of the terrane (Canil *et al.*, 2003; Johnston *et al.*, 2007). U-Pb zircon crystallization ages of 261.5 ± 2.3 Ma from an associated leucogabbro, and 262.3 ± 0.4 Ma from an emplacement-related migmatite derived from the YTT metasedimentary rock which hosts the peridotite (Figure 10), mark the timing of peridotite emplacement during extension and exhumation of YTT (Canil *et al.*, 2003; Johnston *et al.*, 2007). This occurred contemporaneously with exhumation of blueschists and eclogites within the east margin of YTT (Figure 10) (e.g. Erdmer *et al.*, 1998; Fallas *et al.*, 1998).

The Klondike magmatic cycle is recorded by granitic plutons (Figure 1) and associated volcanics (collectively referred to as the Klondike assemblage) within YTT between ~265 and 252 Ma (Figure 10) in Yukon, northern British Columbia and eastern Alaska (e.g. Harms, 1985; Gabrielse *et al.*, 1993; Nelson & Friedman, 2004; Liverton *et al.*, 2005; Murphy *et al.*, 2006; Colpron *et al.*, 2006a; Dusel-Bacon *et al.*, 2006; Nelson *et al.*, 2006 and Beranek & Mortensen, 2011). Beranek and Mortensen (2011) argued for syn-tectonic subduction-related magmatism, deformation and metamorphism between 260 and 254 Ma and post-tectonic magmatism between 254 and 252 Ma. However, the reported occurrences of deformed and undeformed Klondike magmatic assemblages collated in Figure 10 do not show a distinct phase of post-tectonic magmatism. Instead, metamorphism and deformation of YTT metasedimentary units is recorded between ~260 and ~252 Ma (Figures 1 & 10, Fallas, 1998; Villeneuve *et al.*, 2003; Berman *et al.*, 2007; Staples, 2014), contemporaneous with Klondike cycle magmatism and exhumation of YTT (Figures 9c & 10, Wanless *et al.*, 1978; Htoon, 1981; Erdmer & Armstrong, 1988; Hunt & Roddick, 1988; 1993; Oliver, 1996; Erdmer *et al.*, 1998; Fallas *et al.*, 1998; Breitsprecher & Mortensen 2004; Joyce *et al.*, 2015). Within our proposed tectonic framework, the Klondike magmatic cycle is interpreted as either, (1) exhumation-driven and/or asthenospheric flow-driven crustal melting in response to orogenic collapse (i.e. extension)

after slab break-off (Figure 9b-c) (e.g. Dewey, 1988; Huw Davies & von Blackenburg, 1995; Atherton & Ghani, 2002; Brown *et al.*, 2011; Li *et al.*, 2016), (2) arc-derived magmatism generated in response to initiation of westward subduction beneath the Klondike orogen following slab break-off and subduction polarity reversal (e.g. Stern, 2004); or; (3) a combination of both (1) and (2). All three interpretations fit with geochemical and geochronological constraints from plutonic components of the Klondike magmatic cycle (e.g. Ruks *et al.*, 2006; Beranek & Mortensen, 2011). We also note that magmatism in response to eastward subduction of Panthalassa Ocean beneath YTT cannot be ruled out.

We propose that the events described above occurred in response to buoyancy-driven slab break-off from the subducted margin of YTT continental crust (e.g. Cloos, 1993; Afonso & Zlotnik, 2011) followed by initiation of westward subduction and roll-back of the ocean basin that lay east of the Dunite Peak intra-oceanic arc (e.g. Dewey, 1988; Huw Davies & von Blackenburg, 1995; Atherton & Ghani, 2002; Duretz *et al.*, 2010; Brown *et al.*, 2011). Obduction of SSZ ophiolites of the Dunite Peak intra-oceanic arc on to YTT probably occurred during or soon after these events, whilst they were young (<10 M.yr.) and hot (e.g. Dewey, 2003). The period between 265 and 260 Ma marks the starting point for these events, triggered by the cessation of subduction of YTT (Figure 10), but we note that the relative timing and duration of slab break-off and subduction polarity reversal is poorly constrained and may have taken longer than five million years (e.g. Brown *et al.*, 2011). The latest occurrence of metamorphism of YTT coeval with exhumation and Klondike magmatism marks the final stage of the Klondike orogeny. Thus, we bracket the duration of Klondike orogeny between ~275 and ~252 Ma (Figure 10). This outlined sequence of events is comparable to the evolution of other ancient arc-continent collisions, such as the Grampian, Taconic and Kamchatka arc-continent orogens (e.g. Dewey, 2005; Boutelier & Chemenda, 2011; Brown *et al.*, 2011 and references therein). We also note that the duration of the Klondike orogeny (~20-25 M.yr) is comparable to the duration of other arc-continent collisions (~20-50 M.yr.), as opposed to the longer duration of continent-continent collisions (≥ 50 M.yr.), which would be expected for a collision between YTT and Laurentia (e.g. Friedrich *et al.*, 1999; Dewey, 2005; van Staal *et al.*, 2007; Chew *et al.*, 2010; Brown *et al.*, 2011).

9. REMAINING PROBLEMS AND FUTURE WORK

9.1. Accretion of the Klondike orogen to Laurentia

Our study argues that YTT did not collide with Laurentia during the Permian. Previous studies proposed that deposition of the Jones Lake Formation on YTT, Laurentia and SMT marked the final stages of collision, accretion and related subsidence between YTT and Laurentia, following their collision in the Permian (Colpron *et al.*, 2006; 2007; Beranek & Mortensen, 2011). However, close inspection of variations in detrital zircon populations and conodont fauna within the Jones Lake Formation (*see Section 2.1 for a review of this data*) indicate that these data are at best, consistent with a post-Middle Triassic collision but do not validate, and in some cases are inconsistent with a model of deposition in a regional Triassic basin overlapping YTT, SMT and Laurentia following Permian collision (e.g. Colpron *et al.*, 2007; Beranek *et al.*, 2010; Beranek & Mortensen, 2011). We also note that the widespread Late Triassic to Middle Jurassic plutons and Permian and Jurassic high-grade metamorphism recorded within YTT are absent from Laurentia in Yukon (e.g. Berman *et al.*, 2007; Staples *et al.*, 2014; Colpron *et al.*, 2016b).

The present day lithospheric structure of the Northern Cordillera suggests that YTT forms an overriding thrust sheet emplaced on top of Laurentia (e.g. Gordey, 2002; Cook *et al.*, 2004; Calvert *et al.*, 2017). To satisfy this constraint, we suggest that after the Klondike orogeny, oceanic lithosphere that lay between Laurentia and the Dunite Peak intra-oceanic arc was subducted westward beneath the Klondike orogen (Figure 9d). We propose that the Jones Lake Formation represents accreted remnant ocean plate stratigraphy (magenta accretionary complex, Figure 9c-d) and/or forearc/passive margin basin sediments (e.g. Gordey, 2013) deposited in the basin between the Klondike orogen and Laurentia (e.g. Ingersole, 1988; Ingersole *et al.*, 2003), which closed sometime after the Middle Triassic (e.g. Hansen *et al.*, 1991; Stevens *et al.*, 1996; Plint & Gordon, 1997; Hansen and Dusel-Bacon 1998; Gordey, 2002, 2013). This is consistent with the occurrence of unimodal/bimodal Permian-Triassic \pm Devonian – Early Mississippian detrital zircon populations (Beranek & Mortensen, 2011) and “exotic” Tethyan conodont species (Orchard, 2006) in Middle to Late Triassic strata that overlie parts of SMT Yukon and northern British Columbia. Additionally, paleomagnetic analysis of red chert units of SMT (Richards *et al.*, 1993), suggested that parts of SMT remained allochthonous with respect to Laurentia until the Early Jurassic (*see Section 2.1.*). We propose that

these red chert units derived from the basin between the Dunite Peak intra-oceanic arc and the Laurentian margin.

The exact timing of collision between Laurentia and the Klondike orogen is unclear. Early Jurassic amphibolite facies metamorphism followed by Early to Middle Jurassic exhumation recorded within YTT in Canada and eastern Alaska may record collision between Laurentia and the Klondike orogen and its subsequent collapse (e.g. Dusel-Bacon *et al.*, 2002; Berman *et al.*, 2007; Joyce *et al.*, 2015; Morneau, 2017; Morneau *et al.*, 2017). However, Jurassic metamorphism and exhumation within YTT have also been interpreted as a record of collision and accretion between YTT and Stikinia-Quesnellia (e.g. Colpron *et al.*, 2015; Clark, 2017). Collision between YTT-Stikinia and the Insular terranes (Alexander-Wrangellia, Figure 1) is hypothesized during the Early to Middle Jurassic (Monger, 2014) or the Late Jurassic to Cretaceous (Sigloch & Mihalynuk, 2017). The timing of collision and accretion and the polarity of subduction zones responsible for accretion between the Intermontane terranes (YTT-Stikinia-Quesnellia), the Insular terranes and Laurentia is still debated (e.g. Johnston, 2008; Hildebrand, 2009; Monger, 2014; Sigloch & Mihalynuk, 2017).

The distribution of Early Cretaceous plutonic suites emplaced within both YTT and Laurentia (e.g. Colpron *et al.*, 2016b) provides a latest constraint on this collision and accretion, suggesting that YTT had accreted to Laurentia by ~120 Ma. Emplacement of Early Cretaceous plutons into YTT and Laurentia (e.g. Colpron *et al.*, 2016b) was contemporaneous with amphibolite facies metamorphism of the underlying Laurentian margin (e.g. Gibson *et al.*, 2008; Moynihan, 2013; Staples *et al.*, 2016; Ryan *et al.*, 2017). This has led some authors to propose that the allochthonous terranes first accreted with each other before accreting to Laurentia sometime during the Cretaceous (e.g. Johnston, 2008; Hildebrand, 2009).

Integration of our study with existing datasets indicates that that collision and accretion between the Klondike orogen and Laurentia occurred *after* the Middle Triassic (e.g. Hansen *et al.*, 1991; Richards *et al.*, 1993; Stevens *et al.*, 1996; Plint & Gordon, 1997; Hansen and Dusel-Bacon 1998; Gordey, 2002, 2013), and perhaps as late as post-Jurassic (e.g. Johnston, 2008; Hildebrand, 2009). However, the variability of timing estimates and subduction zone polarity models hypothesized by previous studies (described above),

demonstrates that the timing, order and sequence of collisions between the allochthonous terranes and Laurentia that occurred after the Klondike orogeny requires further investigation. The disruption and/or displacement of original emplacement structures associated with the Permian subduction zone beneath the Dunite Peak intra-oceanic arc occurred during one or more of the subsequent collisional events listed above.

9.2. Re-assessment of the Slide Mountain terrane

Within our model we make a clear argument that the DPO and other correlative SSZ ophiolites derive from the upper plate of the Dunite Peak intra-oceanic arc. Less certain, is the identification of ocean plate stratigraphy (OPS) derived from the lower plate that subducted beneath this intra-oceanic arc or from the basin between the Dunite Peak intra-oceanic arc and Laurentia. We suggest that early Permian and older occurrences of SMT may represent accreted remnants of OPS from the subducting oceanic plate that was attached to the east continental margin of YTT. These comprise supracrustal sections of basinal sedimentary rocks and associated mafic volcanics with mid-ocean ridge and/or within-plate geochemical signatures, such as parts of the Campbell Range basalts in the Finlayson Lake district (Figure 1c, Murphy et al., 2006; Piercy et al., 2012). As our model predicts that the basin between the Dunite Peak intra-oceanic arc and Laurentia closed following the Klondike orogeny, OPS attached to the passive margin of Laurentia should be capped by Triassic and younger sediments that are possibly represented by the Jones Lake Formation (*see Section 9.1.*).

Our model also predicts structural separation between remnants of mid-Permian SSZ ophiolites, Mississippian to Permian OPS attached to YTT, and Mississippian to Triassic or younger OPS from the basin between the Dunite Peak intra-oceanic arc and Laurentia. In our study area, the single outcrop of pillow basalt from the marine metasedimentary succession with an E-MORB geochemical signature (Group 4) may be one such example of this lower-plate accreted OPS. Elsewhere, a possible example of structurally distinct elements of SMT is presented in the Finlayson Lake district (Figure 1c) where SMT containing N-MORB, and BABB geochemical signatures appears to be structurally separated from SMT containing N-MORB, E-MORB and OIB (Murphy et al., 2006, *their Figure 16*).

As our study is the first to predict these structurally distinct elements of OPS within SMT, it is difficult to identify these elements of SMT from previous work without reliable age and geochemical constraints. Furthermore, it is likely that subsequent deformation during the Jurassic and Cretaceous (e.g. Staples *et al.*, 2016) overprinted or removed original emplacement-related structural relationships. Further work should be conducted to robustly identify and distinguish between our three predicted elements of SMT. Based on their distinct age, lithology and structural separation from other parts of SMT, we suggest that all upper-plate assemblages associated with the Dunite Peak intra-oceanic arc be recognized as a distinct terrane (e.g. Coney *et al.*, 1981; Ryan *et al.*, 2015).

9.3. Spatial and temporal extent of the Dunite Peak intra-oceanic arc

We encourage further work to investigate its spatial and temporal extent of the Dunite Peak intra-oceanic arc. Our model requires that following the Klondike orogeny, westward subduction of the ocean basin between the Klondike orogen and Laurentia occurred so that they could collide sometime after the Middle Triassic (*see Section 9.1.*). A potential caveat of this hypothesis is the relatively low abundance of Triassic arc-magmatic rocks within YTT (e.g., the Stikine suite, Colpron *et al.*, 2016b). Although we can only speculate, a potential solution is that the magmatic response to westward-subduction of the ocean basin between the Klondike orogen and Laurentia may be recorded by the Triassic Quesnel intra-oceanic arc (see review of Nelson *et al.*, 2013). This would imply that the Quesnel intra-oceanic arc formed on or close to the eastern margin of the Klondike orogen, as a successor arc to the Dunite Peak intra-oceanic arc. Other potentially misidentified correlatives of the Dunite Peak intra-oceanic arc may include greenstone from the Klinkit intra-oceanic arc, which is currently considered part of YTT (e.g. Colpron *et al.*, 2006; Nelson *et al.*, 2013), and yet yielded a U-Pb igneous age of 281 ± 2 Ma and juvenile ($\mathcal{E}_{Nd} = +6.7$ to $+7.4$) IAT geochemical signatures (Roots *et al.*, 2002; Simard *et al.*, 2002). Similarly, recent study of the Permian Nahlin ophiolite, currently assigned to the Cache Creek terrane, also calls for the presence of a previously unrecognized Permian-Triassic intra-oceanic arc that is allochthonous to the intermontane terranes (McGoldrick *et al.*, 2017). Based on our recognition of the Dunite Peak intra-oceanic arc and its similarity with other intra-oceanic arcs in the Northern Cordillera, plus our prediction of two structurally confined OPSs within SMT

that are distinct from each other and the Dunite Peak intra-oceanic arc, we suggest that the current tectonostratigraphic framework of terranes and assemblages in the Northern Cordillera be re-evaluated.

10. CONCLUSIONS

This study demonstrates the importance of identifying and distinguishing between upper-plate and lower-plate components when attempting to understand the tectonic evolution of an accretionary orogen. We have applied this concept to our study of the Dunite Peak ophiolite in south-central Yukon and other previously studied mid-Permian ophiolites in Alaska, Yukon and British Columbia. Our findings indicate that a new explanation is required for the late Paleozoic to early Mesozoic tectonic interaction between of the Yukon-Tanana terrane, Slide Mountain terrane and Laurentian margin of the Northern Cordillera.

The Dunite Peak ophiolite (DPO) forms klippen of mafic-ultramafic strata structurally emplaced over metasedimentary rocks of Yukon-Tanana terrane (YTT). Field structural, geochemical and geochronological analyses conducted on the DPO and underlying metasedimentary strata yield the following conclusions:

- 1) Whole-rock geochemical and Sm-Nd isotopic analyses of mafic-ultramafic assemblages from the DPO identify 5 distinct geochemical groups. Groups 1-3 correspond to arc (Groups 1-2 = IAT to CA) and back-arc (Group 3 = BABB) magmatic components of a SSZ ophiolite formed in the upper plate of an intra-oceanic arc ($\mathcal{E}_{Nd} = +7.2$ to $+9.0$). Group 5 corresponds to highly depleted mantle/lower crustal ultramafic cumulates, formed in a SSZ setting. The geochemical signatures from these groups are comparable to those derived from modern day intra-oceanic arcs, such as the Izu-Bonin, Mariana and Kermadec arcs and Lau basin, in the SW Pacific Ocean. Group 4 corresponds to E-MORB pillow basalt with no record of interaction with a subduction zone and may therefore be tectonically unrelated to the DPO.

- 2) U-Pb zircon geochronology of an IAT gabbro from the DPO yielded a mean igneous crystallization age of 265 ± 4 Ma.

- 3) Geochemical and geochronological constraints correlate the DPO with other mid-Permian (275-260 Ma) ophiolites previously assigned to Slide Mountain terrane (SMT). These correlatives include Quartzrock Creek gabbro, Cassiar block, Zus Mountain block and Blue Mountain block (northern British Columbia, Sylvester allochthon), St Cyr klippe and Tower Peak assemblage and the Finlayson Lake greenstones and

gabbros (south-central Yukon), Tummel fault zone and Ragged Lake klippe (central Yukon), Clinton Creek ophiolite (west Yukon) and the Wolf Mountain klippe (east Alaska) (Figure 1). Together, these ophiolites represent the dismembered upper-plate remnants of a regionally extensive intra-oceanic arc active between YTT and Laurentia during the mid-Permian (~280-260 Ma). We name this arc the *Dunite Peak intra-oceanic arc*.

4) We propose that the Klondike orogeny records deformation, metamorphism and magmatism associated with mid-Permian eastward subduction and collision of YTT beneath the Dunite Peak intra-oceanic arc. Subduction of YTT and associated intra-oceanic arc magmatism terminated at ~265-260 Ma. This was accompanied/followed by slab break-off, orogenic collapse and associated magmatism, and the initiation of westward subduction (present coordinates) beneath the east margin of the Klondike orogen (composite of YTT and the Dunite Peak intra-oceanic arc) between ~265 and ~252 Ma. During this time, the Klondike magmatic cycle occurred in response to either: (1) exhumation-driven crustal melting; (2) newly initiated westward subduction; or (3) a combination (1) and (2).

5) Accretion of the Klondike orogen with Laurentia occurred after the Permian, and probably after the Middle Triassic. This is supported by reassessment of detrital zircon populations and conodont fauna with Triassic sedimentary rocks on YTT, SMT and Laurentia, and the distribution of Triassic to Early Jurassic metamorphism, magmatism and exhumation within YTT that is not record by Laurentia.

6) Mid-Permian SSZ ophiolites of the Dunite Peak intra-oceanic arc are distinct from older supracrustal sections of SMT that formed in an intra-plate/mid-ocean spreading ridge setting. The definition of SMT should be modified to formally recognize the distinction between mid-Permian SSZ ophiolites from older SMT sections. Other parts of SMT may be subdivided into accreted ocean plate stratigraphy derived from (1) the oceanic lower plate attached to YTT that subducted beneath the Dunite Peak intra-oceanic arc and (2) the ocean basin which formed between the Dunite peak intra-oceanic arc and Laurentia. The latter should contain younger strata (post-Permian) than the former. This younger lower plate material from the basin between the Dunite Peak intra-oceanic arc and Laurentia may include the Triassic Jones Lake Formation. The Dunite Peak intra-oceanic arc should be recognized as a distinct terrane and that the current

tectonostratigraphic framework of terranes and assemblages in the Northern Cordillera should be re-evaluated.

Acknowledgements

This research has received funding from the Geological Survey of Canada, GEM-II Cordillera project and the European Research Council (ERC) under the European Union's Horizon 2020 research and innovation programme (grant agreement 639003 "DEEP TIME"). We thank Brad Singer (science editor), John Waldron (ass. editor), John Wakabayashi, Cynthia Dusel-Bacon and Steve Johnston for constructive reviews. JoAnne Nelson (BCGS) is thanked for helpful discussion during initial write-up. Dejan Milidragovic (BCGS) is thanked for guidance during initial interpretations of geochemical data. We thank Shuangquan Zhang (Carlton University) for the Sm-Nd isotopic analyses presented in this study. We thank Capital Helicopters Inc. and the Yukon Geological Survey for logistical support during fieldwork.

References

- Afonso, J.C., Zlotnik, S. 2011. The subductability of continental lithosphere: the before and after story. *In*: Brown, D. & Ryan, P.D. (eds.) *Arc-Continent Collision*. Berlin, Heidelberg: Springer Berlin Heidelberg, p. 53-86.
- Arndt, N.T., Goldstein, S.L. (1989). An open boundary between lower continental crust and mantle: its role in crust formation and crustal recycling. *Tectonophysics*, 161, 201-212.
- Atherton, M.P., Ghani, A.A. (2002). Slab breakoff: a model for Caledonian, Late Granite syn-collisional magmatism in the orthotectonic (metamorphic) zone of Scotland and Donegal, Ireland. *Lithos*. 62, 65-85.
- Barth, A.P., Wooden, J.L. (2006). Timing of Magmatism following Initial Convergence at a Passive Margin, Southwestern U.S. Cordillera, and Ages of Lower Crustal Magma Sources. *The Journal of Geology*. 114, 231-245.
- Barth, A.P., Wooden, J.L. (2010). Coupled elemental and isotopic analyses of polygenetic zircons from granitic rocks by ion microprobe, with implications for melt evolution and the sources of granitic magmas. *Chemical Geology*. 277, 149-159.
- Beranek, L.P. 2009. Provenance and paleotectonic setting of North American Triassic strata in Yukon: the sedimentary record of pericratonic terrane accretion in the northern Canadian Cordillera. [*PhD Thesis*], University of British Columbia, Vancouver, BC, Canada, 338.
- Beranek, L.P., Mortensen, J.K. (2011). The timing and provenance record of the Late Permian Klondike orogeny in northwestern Canada and arc-continent collision along western North America. *Tectonics*. 30, TC5017.
- Beranek, L.P., Mortensen, J.K., Orchard, M.J., Ullrich, T. (2010). Provenance of North American Triassic strata from west-central and southeastern Yukon: correlations with coeval strata in the Western Canada Sedimentary Basin and Canadian Arctic Islands. *Canadian Journal of Earth Sciences*. 47, 53-73.
- Berman, R.G., Ryan, J.J., Gordey, S.P., Villeneuve, M. (2007). Permian to Cretaceous polymetamorphic evolution of the Stewart River region, Yukon-Tanana terrane, Yukon, Canada: P-T evolution linked with in situ SHRIMP monazite geochronology. *Journal of Metamorphic Geology*. 25, 803-827.
- Bézos, A., Escrig, S., Langmuir, C.H., Michael, P.J., Asimow, P.D. 2009. Origins of chemical diversity of back-arc basin basalts: A segment-scale study of the Eastern Lau Spreading Center. *Journal of Geophysical Research: Solid Earth*, B114.
- Bizimis, M., Salters, V.J., Bonatti, E. (2000). Trace and REE content of clinopyroxenes from supra-subduction zone peridotites. Implications for melting and enrichment processes in island arcs. *Chemical Geology*, 165, 67-85.

- Black, L.P., Kamo, S.L., Allen, C.M., Davis, D.W., Aleinikoff, J.N., Valley, J.W., Mundil, R., Campbell, I.H., Korsh, R.J., Williams, I.S., Foudoulis, C. (2004). Improved $^{206}\text{Pb}/^{238}\text{U}$ microprobe geochronology by the monitoring of a trace–element–related matrix effect; SHRIMP, ID–TIMS, ELA–ICP–MS and oxygen isotope documentation for a series of zircon standards. *Chemical Geology*. 205, 115-140.
- Breitsprecher, K., Mortensen, J.K. (2004). *YukonAge 2004 - A database of isotopic age determinations for rock units in Yukon Territory*. Yukon Geological Survey, CD-ROM.
- Boutelier, D. & Chemenda, A. 2011. Physical Modeling of Arc–Continent Collision: A Review of 2D, 3D, Purely Mechanical and Thermo-Mechanical Experimental Models. *In*: Brown, D. & Ryan, P.D. (eds.) *Arc-Continent Collision*. Berlin, Heidelberg: Springer Berlin Heidelberg, p. 445-473.
- Brown, D., Ryan, P.D., Afonso, J.C., Boutelier, D., Burg, J.P., Byrne, T., Calvert, A., Cook, F., Debari, S., Dewey, J.F., Gerya, T.V., Harris, R., Herrington, R., Konstantinovskaya, E., Reston, T. & Zagorevski, A. 2011. Arc–Continent Collision: The Making of an Orogen. *In*: Brown, D. & Ryan, P.D. (eds.) *Arc-Continent Collision*. Berlin, Heidelberg: Springer Berlin Heidelberg, p. 477-493.
- Cabanis, B., Lecolle, M. (1989). Le diagramme La/10-Y/15-Nb/8: un outil pour la discrimination des series volcaniques et la mise en evidence des processys de melange et/ou de contamination crustale. *Comptes Rendus de l'Académie des Sciences-Serie II*. 309, 2023-2029.
- Canil, D., Johnston, S.T., Evers, K., Shellnutt, J.G., Creaser, R.A. (2003). Mantle exhumation in an early Paleozoic passive margin, northern Cordillera, Yukon. *The Journal of Geology*, 111, 313-327
- Cann, J.R. (1970). Rb, Sr, Y, Zr and Nb in some ocean floor basaltic rocks. *Earth and Planetary Science Letters*. 10, 7-11.
- Calvert, A.J., Hayward, N., Vayavur, R. & Colpron, M. 2017. Seismic and gravity constraints on the crustal architecture of the Intermontane terranes, central Yukon. *Canadian Journal of Earth Sciences*, 54, 798-811.
- Cawood, P.A., Suhr, G. 1992. Generation and obduction of ophiolites: Constraints from the Bay of Islands Complex, western Newfoundland. *Tectonics*, 11, 884-897.
- Chew, D.M., Daly, J.S., Magna, T., Page, L.M., Kirkland, C.L., Whitehouse, M.J., Lam, R., 2010. Timing of ophiolite obduction in the Grampian orogen. *GSA Bulletin*, 122, 1787-1799.
- Clark, A.D. 2017. Tectonometamorphic history of mid-crustal rocks at Aishihik Lake, southwest Yukon. [MSc Thesis], pp. 153. Simon Fraser University, Burnaby, BC, Canada.
- Cloos, M. (1993). Lithospheric buoyancy and collisional orogenesis: Subduction of oceanic plateaus, continental margins, island arcs, spreading ridges, and seamounts. *GSA Bulletin*, 105, 715–737.

- Cole, F., Butler, R.F., Gehrels, G.E. (1992). Paleomagnetism of late Paleozoic rocks in the northern Cache Creek terrane near Atlin, British Columbia. *Canadian Journal of Earth Sciences*, 29, 486-498.
- Colpron, M., Gladwin, K., Johnston, S.T., Mortensen, J.K., Gehrels, G.E. (2005). Geology and juxtaposition history of the Yukon-Tanana, Slide Mountain, and Cassiar terranes in the Glenlyon area of central Yukon. *Canadian Journal of Earth Sciences*. 42, 1431-1448.
- Colpron, M., Nelson, J., Murphy, D.C. (2006a). A tectonostratigraphic framework for the pericratonic terranes of the northern Canadian Cordillera. In: Colpron, M., Nelson, J.L. (eds.) *Paleozoic evolution and metallogeny of pericratonic terranes at the ancient Pacific margin of North America, Canadian and Alaskan Cordillera: Geological Association of Canada Special Paper*. 45, 1-23.
- Colpron, M., Mortensen, J.K., Gehrels, G.E., Villeneuve, M. (2006b). Basement complex, Carboniferous magmatism and Paleozoic deformation in Yukon-Tanana terrane of central Yukon: Field, geochemical and geochronological constraints from Glenlyon map area. In: Colpron, M., Nelson, J.L. (eds.) *Paleozoic evolution and metallogeny of pericratonic terranes at the ancient Pacific margin of North America, Canadian and Alaskan Cordillera. Edited by M. Colpron and J.L. Nelson. Geological Association of Canada, Special Paper*. 45, 131-151.
- Colpron, M., Nelson, J., Murphy, D.C. (2007). Northern Cordilleran terranes and their interactions through time. *GSA Today*. 17, 4, 1-10.
- Colpron, M., Crowley, J.L., Gehrels, G., Long, D.G.F., Murphy, D.C., Beranek, L., Bickerton, L. (2015). Birth of the northern Cordilleran orogen, as recorded by detrital zircons in Jurassic synorogenic strata and regional exhumation in Yukon. *Lithosphere*. 7, 541-562.
- Colpron, M., Israel, S., Murphy, D., Pigage, L., Moynihan, D. (2016a). Yukon bedrock geology map. *Yukon Geological Survey*, Open File 2016-1, scale 1:1000,000.
- Colpron, M., Israel, S., Friend, M. (2016b). Yukon Plutonic Suites. *Yukon Geological Survey*, Open File 2016-37, scale 1:750000.
- Colpron, M., Carr, S., Hildes, D., Piercey, S. (2017). Geophysical, geochemical and geochronological constraints on the geology and mineral potential of the Livingstone Creek area, south-central Yukon (NTS 105E/8). In: MacFarlane, K.E., Weston, L.H. (eds.) *Yukon Exploration and Geology Overview 2016*. Yukon Geological Survey, 47-86.
- Coney, P.J., Jones, D.L. and Monger, J.W., 1980. Cordilleran suspect terranes. *Nature*, 288, 329-333.

- Cook, F.A., Clowes, R.M., Snyder, D.B., Van Der Velden, A.J., Hall, K.W., Erdmer, P. & Evenchick, C.A. 2004. Precambrian crust beneath the Mesozoic northern Canadian Cordillera discovered by Lithoprobe seismic reflection profiling. *Tectonics*, 23, TC2010.
- Creaser, R.A., Heaman, L.M., Erdmer, P. (1997). Timing of high-pressure metamorphism in the Yukon – Tanana terrane, Canadian Cordillera: constraints from U – Pb zircon dating of eclogite from the Teslin tectonic zone. *Canadian Journal of Earth Sciences*. 34, 709-715.
- Creaser, R.A., Goodwin-Bell, J.-a.S. & Erdmer, P. 1999. Geochemical and Nd isotopic constraints for the origin of eclogite protoliths, northern Cordillera: implications for the Paleozoic tectonic evolution of the Yukon-Tanana terrane. *Canadian Journal of Earth Sciences*, 36, 1697-1709.
- Cui, Y., Miller, D., Nixon, G., Nelson, J.L. (2015). *British Columbia digital geology*. British Columbia Geological Survey, Open File 2015-2.
- De Keijzer, M., Williams, P.F., Brown, R.L. (1999). Kilometre-scale folding in the Teslin zone, northern Canadian Cordillera, and its tectonic implications for the accretion of the Yukon-Tanana terrane to North America. *Canadian Journal of Earth Sciences*. 36, 479-494.
- De Keijzer, M., Williams, P.F., Carr, S.D. (2000). Reflections on Lithoprobe SNORCLE Line 31 in light of the structure of the Teslin zone in the Last Peak area (NTS map 105 E/9), southern Yukon Territory. In: Cook, F., Erdmer, P. (eds.) *Slave – North American Cordillera Lithospheric Evolution (SNORCLE) Transect and Cordilleran Tectonics Workshop Meeting*. Calgary, Alberta. Lithoprobe Report 72: 114–118.
- Dewey, J.F. 1988. Extensional collapse of orogens. *Tectonics*, 7, 1123-1139.
- Dewey, J., 2003, Ophiolites and lost oceans: Rifts, ridges, arcs, and/or scrapings? In: Dilek, Y., Newcomb, S., (eds.), *Ophiolite concept and the evolution of geological thought*. Geological Society of America Special Paper 373, p. 153–158.
- Dewey, J.F. 2005. Orogeny Can Be Very Short. *Proceedings of the National Academy of Sciences of the United States of America*, 102, 15286-15293.
- Dilek, Y., Furnes, H. (2014). Ophiolites and Their Origins. *Elements*. 10, 93-100.
- Duretz, T., Gerya, T.V., May, D.A. 2011. Numerical modelling of spontaneous slab breakoff and subsequent topographic response. *Tectonophysics*, 502, 244-256.

- Dusel-Bacon, C. & Cooper, K.M. 1999. Trace-element geochemistry of metabasaltic rocks from the Yukon-Tanana Upland and implications for the origin of tectonic assemblages in east-central Alaska. *Canadian Journal of Earth Sciences*, 36, 1671-1695.
- Dusel-Bacon, C., Hopkins, M.J., Mortensen, J.K., Williams, I., Heslop, K., Dashevsky, S.S., Bressler, J.R., Day, W.C. (2006). Paleozoic tectonic and metallogenetic evolution of the Yukon-Tanana terrane, east-central Alaska. In: Colpron, M., Nelson, J.L. (eds.) *Paleozoic evolution and metallogeny of pericratonic terranes at the ancient Pacific margin of North America, Canadian and Alaskan Cordillera*. Geological Association of Canada, Special Paper 45, 25-74.
- Dusel-Bacon, C., Day, W.C., Aleinikoff, J.N., 2013. Geochemistry, petrography, and zircon U–Pb geochronology of Paleozoic metaigneous rocks in the Mount Veta area of east-central Alaska: Implications for the evolution of the westernmost part of the Yukon–Tanana terrane. *Canadian Journal of Earth Sciences*, 50, 826-846.
- Enkin, R.J. (2006). Paleomagnetism and the case for Baja British Columbia. Paleogeography of the North American Cordillera: evidence for and against large-scale displacements. In: Haggart, J.W., Enkin, R.J., Monger, J.W.H., (eds.) *Paleogeography of the North American Cordillera: Evidence for and against large-scale displacements*. Geological Association of Canada, Special Paper 46 pp.233-253
- Erdmer, P., Armstrong, R.L. (1988). Permo-Triassic Isotopic Dates for Blueschist, Ross River Area, Yukon. In: Abbott, J.G. (ed.) *Yukon Geology Volume 2*. Exploration & Geological Services Division, Yukon, Indian & Northern Affairs Canada, pp33-36.
- Erdmer, P., Ghent, E.D., Archibald, D.A., Stout, M.Z. (1998). Paleozoic and Mesozoic high-pressure metamorphism at the margin of ancestral North America in central Yukon. *GSA Bulletin*. 110, 615-629.
- Fallas, K.M., Erdmer, P., Archibald, D.A., Heaman, L.M., Creaser, R.A. (1998). The St. Cyr Klippe, south-central Yukon: an outlier of the Teslin tectonic zone? *LITHOPROBE SNORCLE Transect Meeting Report*. 131-138.
- Fallas, K., Erdmer, P., Creaser, R., Archibald, D., Heaman, L. (1999). New terrane interpretation for the St. Cyr klippe, south-central Yukon. *LITHOPROBE SNORCLE Transect Meeting Report*. 130-137.
- Ferri, F. 2009. Geology of the Jones Peak Area (NTS94B/02 and 07), Halfway River map sheet (94B). In: *Geoscience Reports 2009*. B.C. Ministry of Energy, Mines and Petroleum Resources, Victoria, BC. pp. 5–23.
- Ferri, F., Golding, M.L., Mortensen, J.K., Zonneveld, J-P., Orchard, M.J., 2010. Toad Formation (Montney and Doig equivalent) in the northwestern Halfway River map area, British Columbia (NTS 094B/14). In: *Geoscience Reports 2010*, BC Ministry of Energy, Mines and Petroleum Resources, pp 21–34.
- Ferry, J.M., Watson, E.B. (2007). New thermodynamic models and revised calibrations for the Ti-in-zircon and Zr-in-

- rutile thermometers. *Contributions to Mineralogy and Petrology*. 154, 429-437.
- Florio, G., Fedi, M., Cella, F. (2011). Insights on the spreading of the Tyrrhenian Sea from the magnetic anomaly pattern. *Terra Nova*. 23, 127-133.
- Foster, H.L. & Keith, T.E.C. 1974. Ultramafic rocks of the Eagle quadrangle, east-central Alaska: U.S. Geological Survey. *Journal of Research*, 2, 657-669.
- Foster, H.L., Keith, T.E.C., Menzie, W.D. (1994). Geology of the Yukon-Tanana area of east-central Alaska. *In*: Plafker, G., Berg, H.C. (eds.) *The Geology of Alaska*. Geological Society of America, 205–240.
- Friedrich, A.M., Bowring, S.A., Martin, M.W., Hodges, K.V., 1999. Short-lived continental magmatic arc at Connemara, western Irish Caledonides: Implications for the age of the Grampian orogeny. *Geology*, 27, 27-30.
- Gabrielse, H., Mortensen, J.K., Parrish, R.R., Harms, T.A., Nelson, J.L., van Der Heyden, P. (1993). Late Paleozoic plutons in the Sylvester Allochthon, northern British Columbia, Report 7. *In*: *Radiogenic Age and Isotopic Studies*. Geological Survey of Canada. Paper 93-2, 107-118.
- Gabrielse, H., Murphy, D.C., Mortensen, J.K., (2006). Cretaceous and Cenozoic dextral orogen-parallel displacements, magmatism and paleogeography, north-central Canadian Cordillera. *In*: Haggart, J.W., Enkin, R.J., Monger, J.W.H., (eds.) *Paleogeography of the North American Cordillera: Evidence for and against large-scale displacements*. Geological Association of Canada, Special Paper 46, 255-276.
- Gallagher, C. S. (1999). Regional-scale transposition and late large-scale folding in the Teslin Zone, Pelly Mountains, Yukon. [*MSc Thesis*] Carleton University, Ottawa, ON, pp199.
- Gibson, H.D., Brown, R.L., Carr, S.D. (2008). Tectonic evolution of the Selkirk fan, southeastern Canadian Cordillera: A composite Middle Jurassic–Cretaceous orogenic structure. *Tectonics*, 27, TC6007.
- Gilotti, J.A., McClelland, W.C., van Staal, C.R., Petrie, M.B. (2017). Detrital zircon evidence for eclogite formation by basal subduction erosion—An example from the Yukon-Tanana composite arc, Canadian Cordillera. *In*: Bianchini, G., Bodinier, J.-L., Braga, R., Wilson, M. (eds.) *The Crust-Mantle and Lithosphere-Asthenosphere Boundaries: Insights from Xenoliths, Orogenic Deep Sections, and Geophysical Studies*. Geological Society of America Special Paper 526, 173-189.
- Golding, M.L., Mortensen, J.K., Ferri, F., Zonneveld, J.P., Orchard, M.J. 2016a. Determining the provenance of Triassic sedimentary rocks in northeastern British Columbia and western Alberta using detrital zircon geochronology, with implications for regional tectonics. *Canadian Journal of Earth Sciences*, 53, 140-155.
- Golding, M.L., Mortensen, J.K., Zonneveld, J.-P., Orchard, M.J., 2016b. U-Pb isotopic ages of euhedral zircons in the

- 048 Rhaetian of British Columbia: Implications for Cordilleran tectonics during the Late Triassic. *Geosphere*, 12,
049 5, 1606–1616.
- 050 Goodwin-Bell, J.-A. (1998). A geochemical and Sm-Nd isotopic study of Cordilleran eclogites from the Yukon-
051 Tanana terrane. [MSc Thesis] University of Alberta, Edmonton, AB, pp145
- 052 Gordey, S.P. 2002. Is Yukon-Tanana Terrane North America? In: Cook, F. & Erdmer, P. (eds.) *SNORCLE Transect*
053 *and Cordilleran Tectonics Workshop Meeting*. Pacific Geoscience Centre.
- 054 Gordey, S.P. 2013. Evolution of the Selwyn Basin region, Sheldon Lake and Tay River map areas, central Yukon.
055 *Geological Survey of Canada, Bulletin 599*, pp 176.
- 056 Hansen, V.L., Dusel-Bacon, C. (1998). Structural and kinematic evolution of the Yukon-Tanana upland tectonites,
057 east-central Alaska: A record of late Paleozoic to Mesozoic crustal assembly. *GSA Bulletin*. 110, 211-230.
- 058 Hansen, V.L., Heizler, M.T., Harrison, T.M. (1991). Mesozoic thermal evolution of the Yukon-Tanana Composite
059 Terrane: New evidence from $^{40}\text{Ar}/^{39}\text{Ar}$ data. *Tectonics*. 10, 51-76.
- 060 Harms, T.A. 1985. Pre-emplacement thrust faulting in the Sylvester allochthon, northeast Cyr Lake map area, British
061 Columbia. *Geological Survey of Canada, Paper 85-1A*, 301-304.
- 062 Hayden, L.A., Watson, E.B. (2007). Rutile saturation in hydrous siliceous melts and its bearing on Ti-thermometry of
063 quartz and zircon. *Earth and Planetary Science Letters*. 258, 561-568.
- 064 Hildebrand, R.S. (2009). *Did westward subduction cause Cretaceous-Tertiary orogeny in the North American*
065 *Cordillera?*. Geological Society of America Special Paper 457, pp 71.
- 066 Htoon, M. (1981). Isotopic age determinations of some metamorphic and igneous rocks from Clinton Creek area,
067 Yukon. In: Tempelman-Kluit, D.J. (ed.) *Yukon Geology and Exploration 1979-80*. Indian and Northern
068 Affairs Canada, Exploration & Geological Services Division, 65-67.
- 069 Hunt, P.A. & Roddick, J.C. 1988. A compilation of K-Ar ages: Report 18 *Radiogenic Age and Isotopic Studies:*
070 *Report 2*, Geological Survey of Canada Paper 88-2, 127-153.
- 071 Hunt, P.A. & Roddick, J.C. 1993. A compilation of K-Ar and ^{40}Ar - ^{39}Ar ages: report 23. *Radiogenic Age and*
072 *Isotopic Studies: Report 7*, Geological Survey of Canada, Paper 93-2.
- 073 Huw Davies, J., Von Blanckenburg, F. (1995). Slab breakoff: A model of lithosphere detachment and its test in the
074 magmatism and deformation of collisional orogens. *Earth and Planetary Science Letters*. 129, 85-
075 102. Kakegawa, T., Utsumi, M., Marumo, K. (2008), Geochemistry of Sulfide Chimneys and Basement Pillow
076 Lavas at the Southern Mariana Trough (12.55°N–12.58°N). *Resource Geology*, 58, 249–266.
- 077 Ingersoll, R.V. 1988. Tectonics of sedimentary basins. *GSA Bulletin*, 100, 1704-1719.

- Ingersoll, R.V., Dickinson, W.R., and Graham, S.A., 2003, Remnant-ocean submarine fans: Largest sedimentary systems on Earth. *In: Chan, M.A., Archer, A.W., (eds.), Extreme depositional environments: Mega end members in geologic time.* Geological Society of America Special Paper 370, p. 191–208.
- Ishizuka, O., Geshi, N., Kawanabe, Y., Ogitsu, I., Taylor, R.N., Tuzino, T., Sakamoto, I., Arai, K., Nakano, S., 2014. Long-distance magma transport from arc volcanoes inferred from the submarine eruptive fissures offshore Izu-Oshima volcano, Izu–Bonin arc. *Journal of Volcanology and Geothermal Research*, 285, 1-17.
- Isozaki, Y., Maruyama, S., Furuoka, F. (1990). Accreted oceanic materials in Japan. *Tectonophysics*, 181, 179–205
- Keller, N.S., Arculus, R.J., Hermann, J., Richards, S. (2008). Submarine back-arc lava with arc signature: Fonualei Spreading Center, northeast Lau Basin, Tonga. *Journal of Geophysical Research*. 113, B08S07.
- Kimura, J.-I., Gill, J.B., van Keken, P.E., Kawabata, H., Skora, S. (2017). Origin of geochemical mantle components: Role of spreading ridges and thermal evolution of mantle. *Geochemistry, Geophysics, Geosystems*. 18, 697-734.
- Klein, E.M. (2004). Geochemistry of the Igneous Oceanic Crust. *In: Holland, H.D., Turekian, K.K. (Eds.), Treatise on Geochemistry.* Elsevier, Amsterdam. 3, pp. 433-463.
- Kusky, T.M., Windley, B.F., Safonova, I., Wakita, K., Wakabayashi, J., Polat, A., Santosh, M. (2013). Recognition of oceanic plate stratigraphy in accretionary orogens through Earth history: A record of 3.8 billion years of sea floor spreading, subduction, and accretion. *Gondwana Research*, 24, 501–547
- Lin, S., Xing, G., Davis, D.W., Yin, C., Wu, M., Li, L., Jiang, Y., Chen, Z., (2018). Appalachian-style multi-terrane Wilson cycle model for the assembly of South China. *Geology, In Press*.
- Johnston, S.T., Canil, D., Heaman, L.H., 2007. Permian exhumation of the Buffalo Pitts orogenic peridotite massif, northern Cordillera, Yukon. *Canadian Journal of Earth Sciences*, 44, 275-286.
- Johnston, S.T., 2008. The cordilleran ribbon continent of North America. *Annual Review of Earth and Planetary Sciences*, 36, 495-530.
- Joyce, N.L., Ryan, J.J., Colpron, M., Hart, C.J.R., Murphy, D.C. (2015). A compilation of $^{40}\text{Ar}/^{39}\text{Ar}$ age determinations for igneous and metamorphic rocks, and mineral occurrences from central and southeast Yukon. *Geological Survey of Canada, Open File 7924*, pp229.
- Li, S., Chung, S.-L., Wilde, S.A., Wang, T., Xiao, W.-J. & Guo, Q.-Q. 2016. Linking magmatism with collision in an accretionary orogen. *Scientific Reports*, 6, 25751.

- Liverton, T., Mortensen, J.K. & Roots, C.F. 2005. Character and metallogeny of Permian, Jurassic and Cretaceous plutons in the southeastern Yukon-Tanana Terrane. *In*: Emond, D.S., Lewis, L.L. & Bradshaw, G.D. (eds.) *Yukon Exploration and Geology 2004*. Yukon Geological Survey.
- Ludwig, K.R. (2009). SQUID 2, A user's manual (rev 2.50). *Berkeley Geochronology Center Special Publication*. 5, 110.
- Ludwig, K.R. (2012). User's manual for Isoplot 3.75: A geochronological toolkit for Microsoft Excel. *Berkeley Geochronology Center Special Publication*. 5, 75.
- Mann, P., Taira, A., (2004). Global tectonic significance of the Solomon Islands and Ontong Java Plateau convergent zone. *Tectonophysics*, 389, 37-190.
- Matthews, W.A., Guest, B., Coutts, D., Bain, H., Hubbard, S. (2017). Detrital zircons from the Nanaimo basin, Vancouver Island, British Columbia: An independent test of Late Cretaceous to Cenozoic northward translation. *Tectonics*, 36, 854–876.
- Matthews, W., Guest, B., Madronich, L. (2018), Latest Neoproterozoic to Cambrian detrital zircon facies of western Laurentia. *Geosphere*, 14, 243–264.
- Mazdab, F.K., Wooden, J.L. (2006). Trace element analysis in zircon by ion microprobe (SHRIMP-RG): Technique and applications. *Geochimica et Cosmochimica Acta*. 70, A405.
- McDonough, W.F., Frey, F.A. (1989). REE in upper mantle rocks. *In*: Lipin, B., McKay, G.R. (Eds.), *Geochemistry and mineralogy of rare Earth elements*. Mineralogical Society of America, Chelsea, Michigan, pp. 99-145.
- McDonough, W.F., Sun, S.S. (1995). The composition of the Earth. *Chemical Geology*. 120, 223-253.
- McGoldrick, S., Zagorevski, A., Canil, D. (2017). Geochemistry of volcanic and plutonic rocks from the Nahlin ophiolite with implications for a Permo-Triassic arc in the Cache Creek terrane, northwestern British Columbia. *Canadian Journal of Earth Sciences*, *In Press*.
- Mihalynuk, M.G., Friedman, R.M., Devine, F. & Heaman, L.M. 2006. Protolith age and deformation history of the Big Salmon Complex, relicts of a Paleozoic continental arc in northern British Columbia. *In*: Colpron, M. & Nelson, J.L. (eds.) *Paleozoic Evolution and Metallogeny of Pericratonic Terranes at the Ancient Pacific Margin of North America, Canadian and Alaskan Cordillera*. Geological Association of Canada.
- Monger, J.W. (2014). Logan Medallist 1. Seeking the Suture: The Coast-Cascade Conundrum. *Geoscience Canada*, 41, 379-398.
- Morneau, Y.E. 2017. Tectono-Metamorphic Evolution of the Snowcap Assemblage, Yukon-Tanana Terrane, West-Central Yukon. [MSc Thesis], pp. 199. Carleton University, Ottawa, ON., Canada.

- Morneau, Y.E., Gaidies, F., Ryan, J.J. & Zagorevski, A. 2017. Geological Survey of Canada, Current Research 2017-2. 21.
- Mortensen, J.K., 1990. Geology and U–Pb geochronology of the Klondike District, west-central Yukon Territory. *Canadian Journal of Earth Sciences*, 27, 903-914.
- Mortensen, J.K. 1992a. Pre-Mid-Mesozoic tectonic evolution of the Yukon-Tanana Terrane, Yukon and Alaska. *Tectonics*. 11, 836-853.
- Mortensen, J.K. 1992b. New U-Pb ages for the Slide Mountain terrane in southeastern Yukon Territory. *Radiogenic Age and Isotopic Studies, Report 5: Geological Survey of Canada*.
- Moynihan, D.P. (2013). A preliminary assessment of low pressure, amphibolite-facies metamorphism in the upper Hyland River area (NTS 105H), southeast Yukon. *In: MacFarlane, K.E., Nordling, M.G., Sack, P.J. (eds.), Yukon Exploration and Geology 2012*, Yukon Geological Survey, 99-114.
- Murphy, D.C., Colpron, M., Roots, C.F., Gordey, S.P., and Abbott, J.G., 2002, Finlayson Lake Targeted Geoscience Initiative (southeastern Yukon), Part 1: Bedrock geology. *In: Emond, D.S., Weston, L.H., Lewis, L.L., (eds.), Yukon Exploration and Geology 2001*, Exploration and Geological Services Division, Yukon Region, Indian and Northern Affairs Canada, p. 189-207.
- Murphy, D.C., Mortensen, J.K., Piercey, S.J., Orchard, M.J., Gehrels, G.E. (2006). Mid-Paleozoic to early Mesozoic tectonostratigraphic evolution of Yukon-Tanana and Slide Mountain terranes and affiliated overlap assemblages, Finlayson Lake massive sulphide district, southeastern Yukon. *In: Colpron, M., Nelson, J.L. (eds.) Paleozoic evolution and metallogeny of pericratonic terranes at the ancient Pacific margin of North America, Canadian and Alaskan Cordillera*. Geological Association of Canada. Special Paper 45, 75-105.
- Nelson, J.L. (1993). The Sylvester Allochthon: upper Paleozoic marginal-basin and island-arc terranes in northern British Columbia. *Canadian Journal of Earth Sciences*. 30, 631-643.
- Nelson, J.L., Bradford, J. (1993). Geology of the Midway-Cassiar area, northern British Columbia. *B.C. Ministry of Energy, Mines and Petroleum Resources, Bulletin* 83. 94.
- Nelson, J.L. 1999. Devono-Mississippian VMS Project: Continuing Studies in the Dorsey Terrane, Northern British Columbia. *B.C. Ministry of Energy and Mines, Geological Fieldwork 1998*, Paper 1999-1, 143-155.
- Nelson, J.L. 2001. Geology of North-Central Jennings River Area (104O/14E, 15). *B.C. Ministry of Energy and Mines, Geological Fieldwork 2000*, Paper 2001-1, 51-66.
- Nelson, J.L. & Lepage, L.D. 2002. Geology of North-central Jennings River Map Area (NTS 104O/14E, 15). *B.C. Ministry of Energy and Mines Open File 2001-06*, 1:50,000 scale.

- Nelson, J., Friedman, R. (2004). Superimposed Quesnel (late Paleozoic–Jurassic) and Yukon–Tanana (Devonian–Mississippian) arc assemblages, Cassiar Mountains, northern British Columbia: field, U–Pb, and igneous petrochemical evidence. *Canadian Journal of Earth Sciences*. 41, 1201–1235.
- Nelson, J., Colpron, M., Piercey, S.J., Dusel-Bacon, C., Murphy, D.C., Roots, C.F. (2006). Paleozoic tectonic and metallogenetic evolution of pericratonic terranes in Yukon, northern British Columbia and eastern Alaska. *In: Colpron, M., Nelson, J.L. (eds.) Paleozoic evolution and metallogeny of pericratonic terranes at the ancient Pacific margin of North America, Canadian and Alaskan Cordillera*. Geological Association of Canada. Special Paper 45, 323–360.
- Orchard, M.J. 1991. Late Triassic conodont biochronology and biostratigraphy of the Kunga Group, Queen Charlotte Islands, British Columbia. *In: Woodsworth, G.W. (ed.) Evolution and hydrocarbon potential of the Queen Charlotte Basin, British Columbia*.
- Orchard, M.J. (2006). Late Paleozoic and Triassic conodont faunas of Yukon and northern British Columbia and implications for the evolution of the Yukon–Tanana terrane. *In: Colpron, M., Nelson, J.L. (eds.) Paleozoic evolution and metallogeny of pericratonic terranes at the ancient Pacific margin of North America, Canadian and Alaskan Cordillera*. Geological Association of Canada, Special Paper 45, 229–260.
- Oliver, D.H. (1996). Structural, kinematic, and thermochronologic studies of the Teslin suture zone, south-central Yukon Territory. [*PhD Thesis*], Southern Methodist University, Dallas, TX, pp231.
- Parsons, A.J., Ryan, J.J., Coleman, M., van Staal, C.R. (2017a). The Slide Mountain ophiolite, Big Salmon Range, south-central Yukon: Preliminary results from fieldwork. *In: MacFarlane, K.E., Weston, L.H. (eds.) Yukon Exploration and Geology Overview 2016*. Yukon Geological Survey, 181–196.
- Parsons, A.J., Ryan, J.J., Coleman, M. (2017b). Report of activities, 2017: Dunite Peak area, Big Salmon Range, south-central Yukon: GEM2 Cordillera Project. *Geological Survey of Canada, Open File 8307*, pp 10.
- Pearce, J.A. (1996). A user's guide to basalt discrimination diagrams. *In: Wyman, D.A. (eds.) Trace element geochemistry of volcanic rocks: applications for massive sulphide exploration: Geological Association of Canada, Short Course Notes*. 12, 79–113.
- Pearce, J.A., Stern, R.J., Bloomer, S.H., Fryer, P. 2005. Geochemical mapping of the Mariana arc-basin system: Implications for the nature and distribution of subduction components. *Geochemistry, Geophysics, Geosystems*, 6, Q07006.
- Pearce, J.A. (2008). Geochemical fingerprinting of oceanic basalts with applications to ophiolite classification and the search for Archean oceanic crust. *Lithos*. 100, 14–48.

- Pearce, J.A. (2014). Immobile Element Fingerprinting of Ophiolites. *Elements*. 10, 101-108.
- Petrie, M.B., Gilotti, J.A., McClelland, W.C., van Staal, C., Isard, S.J. (2015). Geologic Setting of Eclogite-facies Assemblages in the St. Cyr Klippe, Yukon–Tanana Terrane, Yukon, Canada. *Geoscience Canada*. 42, 327-350.
- Petrie, M.B., Massonne, H.-J., Gilotti, J.A., McClelland, W.C., van Staal, C. (2016). The P – T path of eclogites in the St. Cyr klippe, Yukon, Canada: Permian metamorphism of a coherent high-pressure unit in an accreted terrane of the North American Cordillera. *European Journal of Mineralogy*, 28, 1-20.
- Philippot, P., Blichert-Toft, J., Perchuk, A., Costa, S., Gerasimov, V. (2001). Lu–Hf and Ar–Ar chronometry supports extreme rate of subduction zone metamorphism deduced from geospeedometry. *Tectonophysics*. 342, 23-38.
- Piercey, S., Colpron, M., (2009). Composition and provenance of the Snowcap assemblage, basement to the Yukon–Tanana terrane, northern Cordillera: Implications for Cordilleran crustal growth. *Geosphere*, 5, 439-464.
- Piercey, S.J., Murphy, D.C., Creaser, R.A. (2012). Lithosphere-asthenosphere mixing in a transform-dominated late Paleozoic backarc basin: Implications for northern Cordilleran crustal growth and assembly. *Geosphere*, 8, 716-739.
- Plint, H.E., Gordon, T.M. (1997). The Slide Mountain Terrane and the structural evolution of the Finlayson Lake Fault Zone, southeastern Yukon. *Canadian Journal of Earth Sciences*. 34, 105-126.
- Richard, P., Shimizu, N., Allègre, C.J. (1976). $^{143}\text{Nd}/^{146}\text{Nd}$, a natural tracer: an application to oceanic basalts. *Earth and Planetary Science Letters*. 31, 269-278.
- Richards, D.R., Butler, R.F., Harms, T.A. (1993). Paleomagnetism of the late Paleozoic Slide Mountain terrane, northern and central British Columbia. *Canadian Journal of Earth Sciences*, 30, 898-1913.
- Rollinson, H.R. (1993). *Using geochemical data: evaluation, presentation, interpretation*, Routledge, Harlow, England, pp352.
- Roots, C.F., Harms, T.A., Simard, R.-L., Orchard, M.J., Heaman, L. (2002). Constraints on the age of the Klinkit assemblage east of Teslin Lake, northern British Columbia. *Geological Survey of Canada, Current Research 2002-A7*, pp 11
- Ruks, T.W., Piercey, S.J., Ryan, J.J., Villeneuve, M.E., Creaser, R.A. (2006). Mid- to late Paleozoic K-feldspar augen granitoids of the Yukon–Tanana terrane, Yukon, Canada: Implications for crustal growth and tectonic evolution of the northern Cordillera. *GSA Bulletin*. 118, 1212-1231.
- Ryan, J.J., Nelson, J.L., van Staal, C.R. (2015). Fieldwork in the Sylvester allochthon, Cassiar Mountains, British Columbia: Investigations of the Rapid River tectonite and the Slide Mountain terrane. *In: Geological*

- 226 *Fieldwork 2014, British Columbia*. Ministry of Energy and Mines, British Columbia Geological Survey Paper
227 2015-1, 113-128.
- 228 Ryan, J.J., Zagorevski, A., Joyce, N.L., Staples, R.D.3, Jones, J.V., Gibson, H.D. 2017. Mid-Cretaceous core
229 complexes in the Northern Cordillera: exposing the parautochthon through a thin flap of allochthonous
230 Yukon-Tanana terrane in western Yukon. *GSA Annual Meeting*, Washington, USA.
- 231 Sarbas, B., Nohl, U., 2008. The GEOROC database as part of a growing geoinformatics network. *In*: Brady, S.R.,
232 Sinha, A.K., Gundersen, L.C. (eds.) *Geoinformatics 2008—Data to Knowledge*, Proceedings: U.S. Geological
233 Survey Scientific Investigations Report 2008-5172, pp. 43.
- 234 Salters, V.J.M., Stracke, A. (2004). Composition of the depleted mantle. *Geochemistry, Geophysics, Geosystems*. 5, 1-
235 27.
- 236 Sigloch, K., Mihalynuk, M.G. (2017). Mantle and geological evidence for a Late Jurassic–Cretaceous suture spanning
237 North America. *GSA Bulletin*, 129, 1489-1520.
- 238 Simard, R.-L., Dostal, J., Roots, C.F. (2003). Development of late Paleozoic volcanic arcs in the Canadian Cordillera:
239 an example from the Klinkit Group, northern British Columbia and southern Yukon. *Canadian Journal of*
240 *Earth Sciences*. 40, 907-924.
- 241 Sleeper, J.D., Martinez, F. (2014). Controls on segmentation and morphology along the back-arc Eastern Lau
242 Spreading Center and Valu Fa Ridge. *Journal of Geophysical Research: Solid Earth*. 119, 1678-1700.
- 243 Sleeper, J.D., Martinez, F., Arculus, R. (2016). The Fonualei Rift and Spreading Center: Effects of ultraslow
244 spreading and arc proximity on back-arc crustal accretion. *Journal of Geophysical Research: Solid Earth*. 121,
245 4814-4835.
- 246 Smith, I.E.M., Price, R.C., Stewart, R.B., Worthington, T.J., (2009). An assessment of the mantle and slab
247 components in the magmas of an oceanic arc volcano: Raoul Volcano, Kermadec arc. *Journal of Volcanology*
248 *and Geothermal Research*, 184, 437-450.
- 249 Stacey, J.S., Kramers, J.D. (1975). Approximation of terrestrial lead isotope evolution by a two-stage model. *Earth*
250 *and Planetary Science Letters*. 26, 207-221.
- 251 Staples, R.D. 2014. Diachronous deformation, metamorphism and exhumation in the northern Canadian Cordillera:
252 revealed from pressure-temperature-time deformation paths of former mid-crustal rocks. [*PhD Thesis*], Simon
253 Fraser University, Burnaby, BC, Canada, 229.
- 254 Staples, R.D., Murphy, D.C., Gibson, H.D., Colpron, M., Berman, R.G., Ryan, J.J. (2014). Middle Jurassic to earliest
255 Cretaceous mid-crustal tectono-metamorphism in the northern Canadian Cordillera: Recording foreland-

- directed migration of an orogenic front. *GSA Bulletin*. 126, 1511-1530.
- Staples, R.D., Gibson, H.D., Colpron, M. & Ryan, J.J. 2016. An orogenic wedge model for diachronous deformation, metamorphism, and exhumation in the hinterland of the northern Canadian Cordillera. *Lithosphere*, 8, 165-184.
- Stern, R.J. 2004. Subduction initiation: spontaneous and induced. *Earth and Planetary Science Letters*, 226, 275-292.
- Stevens, R.A., Erdmer, P., Creaser, R.A., Grant, S.L. (1996). Mississippian assembly of the Nisutlin assemblage: evidence from primary contact relationships and Mississippian magmatism in the Teslin tectonic zone, part of the Yukon–Tanana terrane of south-central Yukon. *Canadian Journal of Earth Sciences*. 33, 103-116.
- Sun, S.S., McDonough, W.F. (1989). Chemical and isotopic systematics of oceanic basalts: implications for mantle composition and processes. In: Saunders, A.D., Norry, M.J. (eds.) *Magmatism in the Ocean Basins*. Geological Society of London Special Publications, 42, 313-345.
- Tamaki, K. (1985). Two modes of back-arc spreading. *Geology*. 13, 475-478.
- Tamura, Y., Ishizuka, O., Stern, R.J., Nichols, A.R.L., Kawabata, H., Hirahara, Y., Chang, Q., Miyazaki, T., Kimura, J.-I., Embley, R.W., Tatsumi, Y. 2014. Mission Immiscible: Distinct Subduction Components Generate Two Primary Magmas at Pagan Volcano, Mariana Arc. *Journal of Petrology*, 55, 63-101.
- Tollstrup, D., Gill, J., Kent, A., Prinkey, D., Williams, R., Tamura, Y., Ishizuka, O., 2010. Across-arc geochemical trends in the Izu-Bonin arc: Contributions from the subducting slab, revisited. *Geochemistry, Geophysics, Geosystems*, 11, Q01X10.
- van Staal, C.R., Whalen, J.B., McNicoll, V.J., Pehrsson, S., Lissenberg, C.J., Zagorevski, A., van Breemen, O., Jenner, G.A., 2007, The Notre Dame arc and the Taconic orogeny in Newfoundland. In: Hatcher, R.D., Jr., Carlson, M.P., McBride, J.H., Martínez Catalán, J.R., (eds.), *4-D Framework of Continental Crust*. Geological Society of America Memoir 200, 511–552.
- van Staal, C.R., Whalen, J.B., Valverde-Vaquero, P., Zagorevski, A., Rogers, N., 2009, Pre-Carboniferous episodic accretion-related, orogenesis along the Laurentian margin of the northern Appalachians. In: Murphy, J.B., Keppie, J.D., Hynes, A.J., (eds.) *Ancient Orogens and Modern Analogues*. Geological Society of London Special Publications, 327, 271–316.
- Villeneuve, M., Ryan, J., Gordey, S., Piercey, S. 2003. *Detailed thermal and provenance history of the Stewart River area (Yukon-Tanana terrane, western Yukon) through application of SHRIMP, Ar-Ar and TIMS*. GAC-MAC-SEG Annual General Meeting, Abstracts Volume 28, page 175, Vancouver, B.C.
- Wakabayashi, J., Dilek, Y. (2000). Spatial and temporal relationships between ophiolites and their metamorphic soles:

- 286 A test of models of forearc ophiolite genesis. *Geological Society of America Special Papers*. 349, 53-64.
- 287 Wakabayashi, J., 2017. Structural context and variation of ocean plate stratigraphy, Franciscan Complex, California:
288 insight into mélangé origins and subduction-accretion processes. *Progress in Earth and Planetary Science*, 4,
289 18.
- 290 Wanless, R.K., Stevens, R.D., Lachance, G.R. & Delabio, R.N. 1978. Age determinations and geological studies, K-
291 Ar isotopic ages, Report 13. *Geological Survey of Canada, Paper 77-2*, 1-60.
- 292 Watson, E.B., Harrison, T.M. (2005). Zircon Thermometer Reveals Minimum Melting Conditions on Earliest Earth.
293 *Science*. 308, 841-844.
- 294 Weissel, J., Reading, H., Stegena, L. (1981). Magnetic lineations in marginal basins of the western Pacific.
295 *Philosophical Transactions of the Royal Society of London A: Mathematical, Physical and Engineering*
296 *Sciences*. 300, 223-247.
- 297 Westberg, E. (2009). Geological map of the 'Mendocina Creek' area (parts of 105E/8 and 105F/5). *Yukon Geological*
298 *Survey, Open File 2009-44*, 1:50 000 scale.
- 299 Westberg, E. (2010). The tectonometamorphic and structural evolution of the Yukon-Tanana and Cassiar terranes in
300 the Mendocina Creek area: Implications for the tectonic framework of south-central Yukon. [BSc Honours]
301 Simon Fraser University, Burnaby, BC, pp147.
- 302 Westberg, E., Colpron, M., Gibson, H.D. (2009). Bedrock geology of western 'Mendocina Creek' (NTS 105F/5) and
303 eastern Livingstone Creek (NTS 105E/8) areas, south-central Yukon. In: Weston, L.H., Blackburn, L.R.,
304 Lewis, L.L. (eds.) *Yukon Exploration and Geology 2008*. Yukon Geological Survey, 227-240.
- 305 Williams, I.S. (1998). U-Th-Pb geochronology by ion microprobe. In: McKibben, M.A., Shanks, W.C., Ridley, W.I.
306 (eds.) *Applications of microanalytical techniques to understanding mineralizing processes - Society of*
307 *Economic Geologists*. Reviews in Economic Geology. 7, 1-35.
- 308 Wilson, B.M. (1989). *Igneous petrogenesis a global tectonic approach*, Springer Science & Business Media, London,
309 UK, pp 466.
- 310 Workman, R.K., Hart, S.R. (2005). Major and trace element composition of the depleted MORB mantle (DMM).
311 *Earth and Planetary Science Letters*. 231, 53-72.
- 312 Wysoczanski, R.J., Wright, I.C., Gamble, J.A., Hauri, E.H., Luhr, J.F., Eggins, S.M., Handler, M.R. 2006. Volatile
313 contents of Kermadec Arc-Havre Trough pillow glasses: Fingerprinting slab-derived aqueous fluids in the
314 mantle sources of arc and back-arc lavas. *Journal of Volcanology and Geothermal Research*, 152, 51-73.

- Wysoczanski, R.J., Todd, E., Wright, I.C., Leybourne, M.I., Hergt, J.M., Adam, C., Mackay, K. (2010). Backarc rifting, constructional volcanism and nascent disorganised spreading in the southern Havre Trough backarc rifts (SW Pacific). *Journal of Volcanology and Geothermal Research*. 190, 39-57.
- Zagorevski, A., van Staal, C.R. (2011). The record of Ordovician arc–arc and arc–continent collisions in the Canadian Appalachians during the closure of Iapetus. *In: Brown, D. & Ryan, P.D. (eds.) Arc-Continent Collision*. Berlin, Heidelberg: Springer Berlin Heidelberg, p. 341-371.
- Zagorevski, A., McNicoll, V.J., Rogers, N., van Hees, G.H. (2015). Middle Ordovician disorganized arc rifting in the peri-Laurentian Newfoundland Appalachians: implications for evolution of intra-oceanic arc systems. *Journal of the Geological Society*. 173, 76-93.

Figure 1. Terrane map of the Northern Cordillera. Modified from Colpron *et al.* (2007). Study area (Dunite Peak ophiolite, DPO) outlined by black box (Figure 2). Inset map (bottom right corner) shows location of Figure 1 with respect to North America. Geochronology localities discussed in this article and synthesized into our new hypothesis are labelled with letters (a) to (o). Age ranges are given for localities with multiple geochronology analyses and correspond to the oldest age plus error and the youngest minus error. Klondike magmatic assemblage (Ass) and correlative units drawn from Cui *et al.* (2015) and Colpron *et al.* (2016a). (a-o) Superscript numbers next to ages correspond to geochronology data sources (discussed in text): (1) Gabrielse *et al.*, 1993, (2) Erdmer *et al.*, 1998, (3) Murphy *et al.* 2006, (4) Mortensen, 1992b, (5) Fallas *et al.*, 1998, (6) Petrie *et al.*, 2015, (7) Petrie *et al.*, 2016, (8) Gilotti *et al.*, 2017, (9) de Keijzer *et al.*, 2000, (10) Creaser *et al.*, 1997, (11) Erdmer & Armstrong, 1988, (12) Godwin-Bell, 1998, (13) Philippot *et al.* 2001, (14) Colpron *et al.*, 2005, (15) Oliver, 1996, (16) Joyce *et al.*, 2015, (17) Johnston *et al.*, 2007, (18) Colpron *et al.*, 2006b, (19) Breitsprecher & Mortensen 2004, (20) Staples, 2014, (21) Berman *et al.*, 2007, (22) Htoon, 1981.

Figure 2. Geological map of the Dunite Peak ophiolite (DPO) with locations of geochronology and geochemistry samples and Figure 3 photo locations. Geochemistry symbols correspond to geochemical groups in Figures 6-7.

Figure 3. (a-b) Photographs of the eastern klippe of the Dunite Peak ophiolite (DPO) with unit boundaries overlain. See Figure 2 and text for map unit descriptions. See Figure 2 for photo locations.

Figure 4. Field images of the Dunite Peak ophiolite (DPO) crustal section. (a) Greenstone volcanoclastic rocks (Group 1 geochemistry) with subordinate chert horizons, lower DPO crustal section. (b) Sheared pillow basalt and greenstone (Group 1a geochemistry) with subordinate sedimentary layers, lower DPO crustal section. (c) Typical lithological representation of volcanic/volcanoclastic greenstone. (d) Typical lithological representation of gabbro (Group 2 geochemistry, upper DPO crustal section). (e) Gabbro (Group 2 geochemistry) intruding fragmental volcanoclastic greenstone, upper DPO crustal section. (f) Gabbro (Group 2 geochemistry) intruding greenstone (Group 1 geochemistry), upper DPO crustal section.

Figure 5. U-Pb geochronology, sample 16RAY-AP074A1 (a) Representative cathodoluminescence (CL) images of zircon grains analyzed and (b) Tera-Wasserburg and (c) chondrite-normalized rare earth element plots of sensitive high-resolution ion microprobe reverse-geometry (SHRIMP-RG) U/Pb and trace element data from sample 16RAY-AP074A1. U/Pb data plotted as 1σ error ellipses uncorrected for common Pb. Black ellipses are used in calculating concordia ages. Weighted mean age uncertainty is reported at the 95% confidence level.

Figure 6. Rare earth element – high field strength element (REE-HFSE) spider diagrams. (a-c) Groups 1-4 normalized against N-MORB (Sun & McDonough, 1989). N-MORB V and Sc concentrations based on Klein (2004). (d) Group 5 normalized against primitive mantle (Sun & McDonough, 1989). Primitive mantle V and Sc concentrations based on McDonough and Frey (1989). Standard REE-HFSE profiles for depleted-MORB mantle (DMM) are displayed for comparison (Salters & Stracke, 2004; Workman & Hart 2005).

Figure 7. Geochemical-tectonomorphic discrimination diagrams. (a) Nb/Y (total alkalinity proxy) vs. Zr/Ti (SiO₂ proxy), based on Pearce (1996). (b) Y-La-Nb ternary discrimination diagram based on Cabanis & Lecolle (1989). (c) Suprasubduction/spreading ridge/within-plate magmatism discrimination diagram (Nb/Yb vs. Th/Yb) based on Pearce (2008, 2014). Black squares show typical values for the magma types indicated by adjacent labels. Vertical arrows represent subduction zone enrichment. (d) Geochemical classification of Group 5 ultramafic samples, based on CIPW normative major element concentrations.

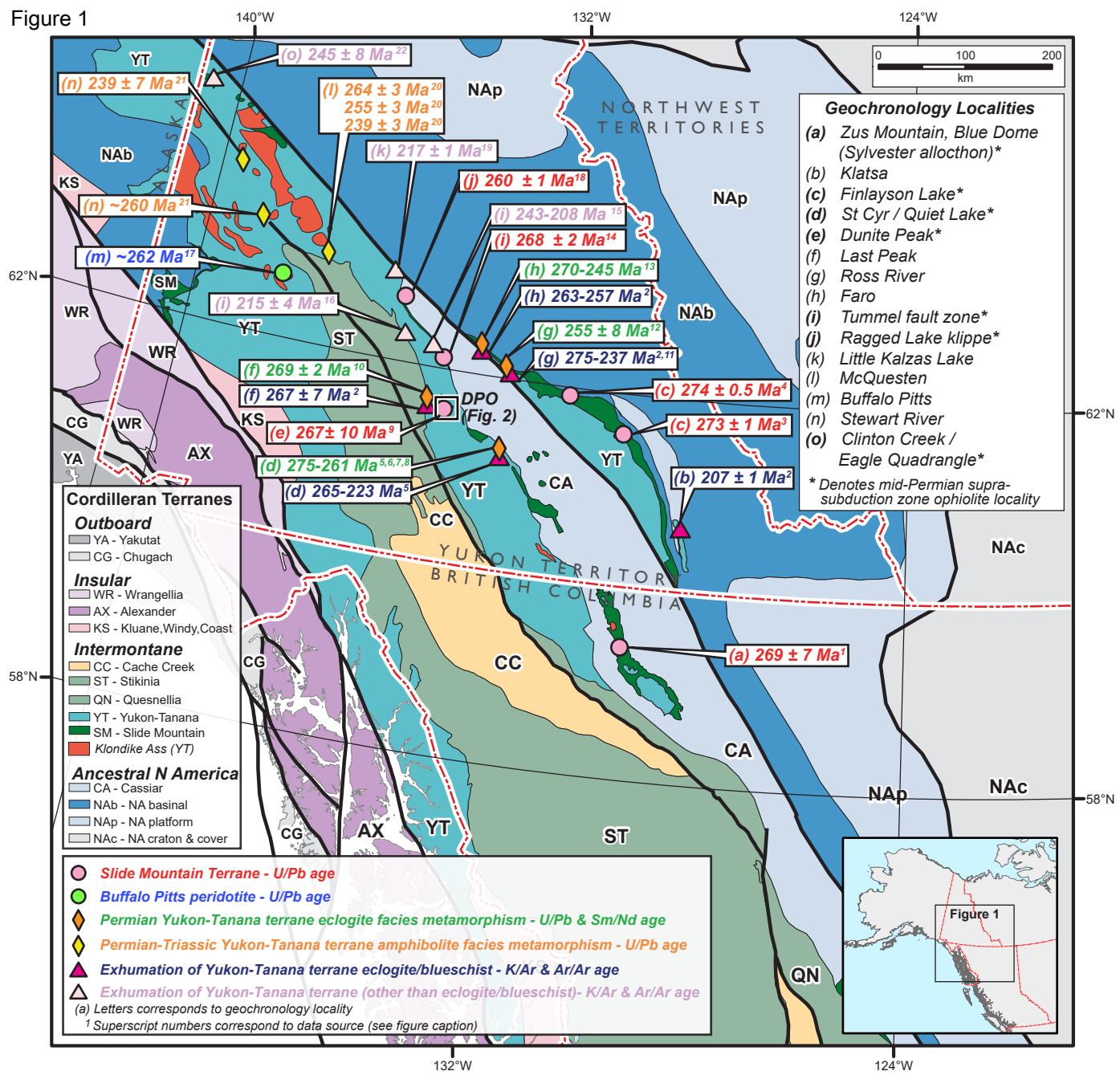
Figure 8. Geochemical signatures of basalt, basaltic andesite and andesite samples collected from active intra-oceanic arcs in the SW Pacific Ocean compared with data collected from the Dunite Peak ophiolite. (a-f) Volcanic glass and whole rock rare earth element – high field strength element (REE-HFSE) concentrations from the Izu-Bonin arc (*red shaded area* – e.g. Tollstrup *et al.*, 2010; Ishizuka *et al.*, 2014), Mariana arc (*orange shaded area* – e.g. Pearce *et al.*, 2005; Tamura *et al.*, 2014), Kermadec arc (*blue shaded area* – e.g. Wysoczanski *et al.*, 2006; Smith *et al.*, 2009) and Lau Basin (*green shaded area* – e.g. Keller *et al.*, 2008; Bézou *et al.*, 2009), drawn from datasets of *n* samples. Data are split into arc samples (a-c) and back-arc/trough/ridge samples (d-e). Note that only data collected from back-arc/trough/ridge settings are available from the Lau Basin (*green shaded area*). Geochemical data from the Dunite Peak ophiolite are delineated with black to grey lined, unshaded areas (g-i) and overlain on SW Pacific data sets for comparison (a-f). Spider diagrams are normalized against N-MORB (Sun & McDonough, 1989). N-MORB V and Sc concentrations based on Klein (2004). Explanation and abbreviations for geochemical-tectonomorphic discrimination diagrams (b-c), (e-f), and (h-i) are same as in Figure 7b-c. Data compiled and extracted from GEOROC database (Sarbas & Nohl, 2008). Full dataset and sources (total of 57 sources) are presented in Supplementary Materials 04.

Figure 9. Cartoon summary of our new model for the Paleozoic–Mesozoic tectonic evolution of the Northern Cordillera, see text for discussion. Yukon-Tanana terrane crust – dark green; YTT eclogite – purple; Laurentian crust – blue; Laurentian margin accretionary complex – magenta; Dunite Peak intra-oceanic arc crust – light grey; Dunite

Peak arc accretionary complex – dark blue; oceanic crust – dark grey; lithospheric mantle – light green; volcanic centres – orange triangles. Not drawn to scale.

Figure 10. Synthesis of isotope geochronology data from Yukon-Tanana terrane (YTT) and the Dunite Peak intra-oceanic arc. Sample numbers (x -axis) correspond to published geochronology data entries in Supplementary Materials 05. Time scale (y -axis) based on Geological Society of America timescale. Data points are divided into specific tectonic processes, labeled in top header, with a color bar to highlight period of activity (e.g. duration of Dunite Peak intra-oceanic arc magmatism indicated by orange bar). Tectonic interpretations of data summarized on right panel. Hatched zone at 265-260 Ma corresponds to cessation of subduction and collision of YTT with the Dunite Peak intra-oceanic arc and the initiation of slab break-off, subduction polarity reversal and associated magmatism. Hatched zone at post-220 Ma marks possible timing of collision and accretion between YTT and Laurentia. See text for discussion.

Figure 1



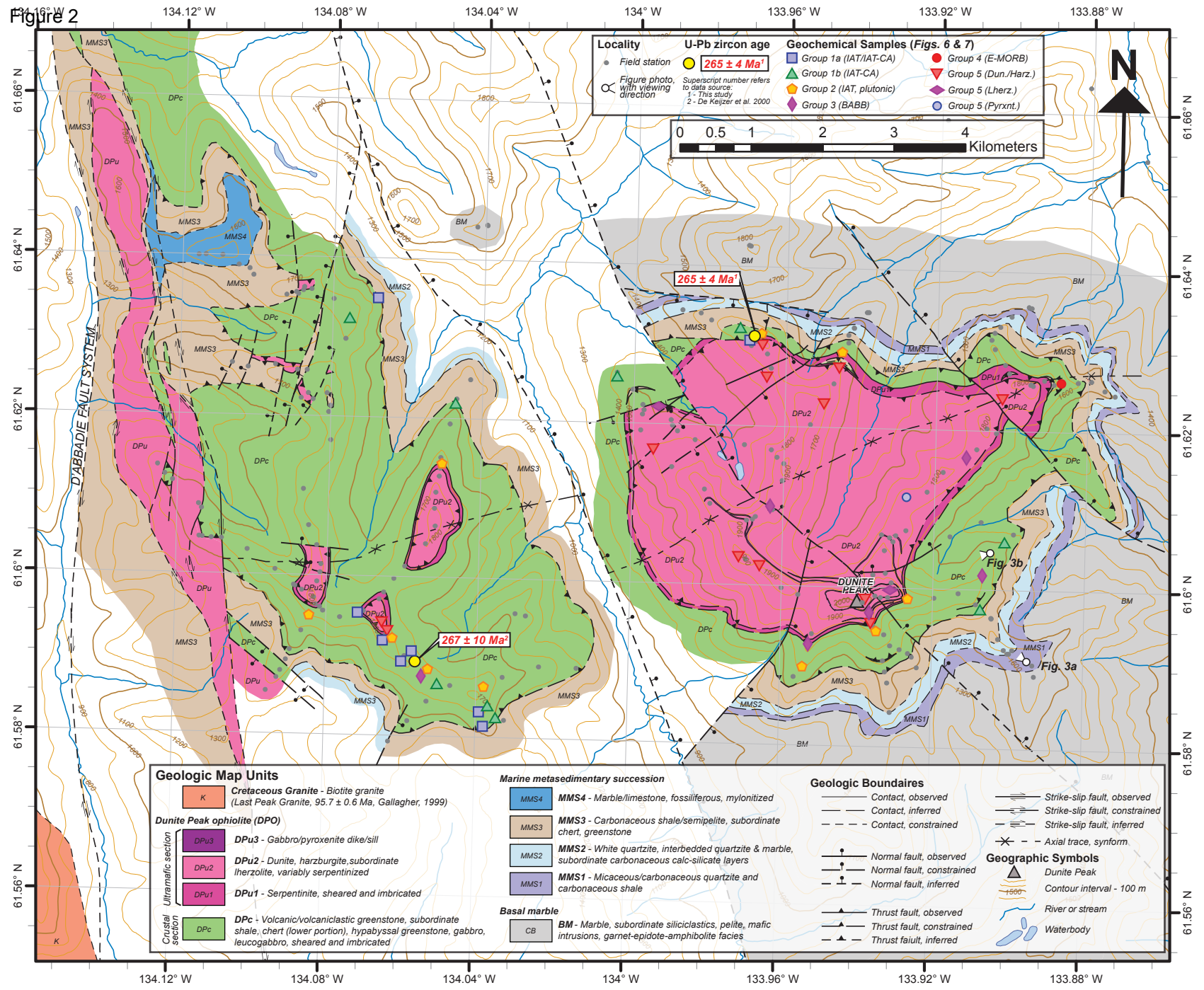


Figure 3

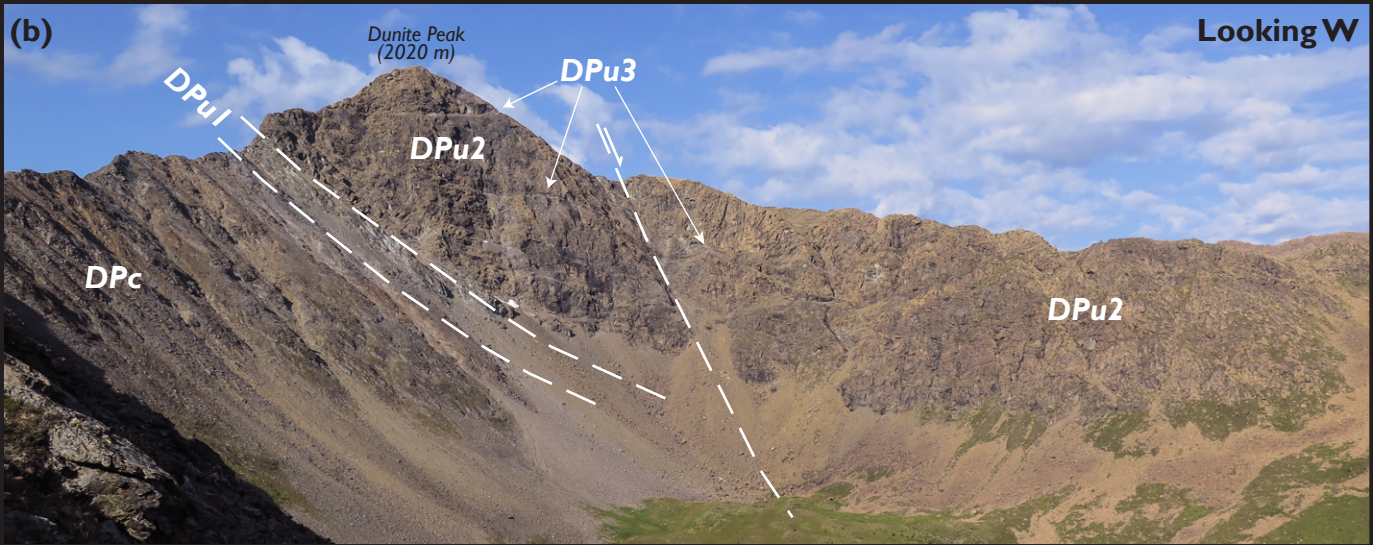
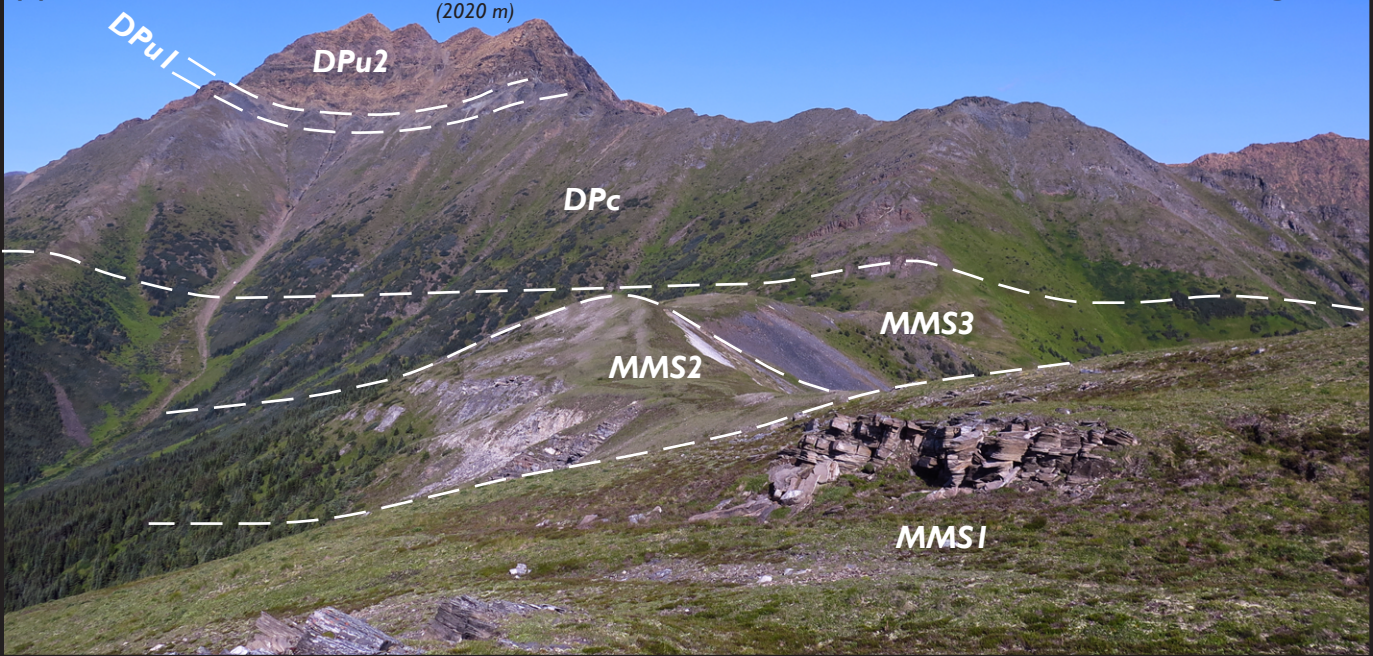


Figure 4

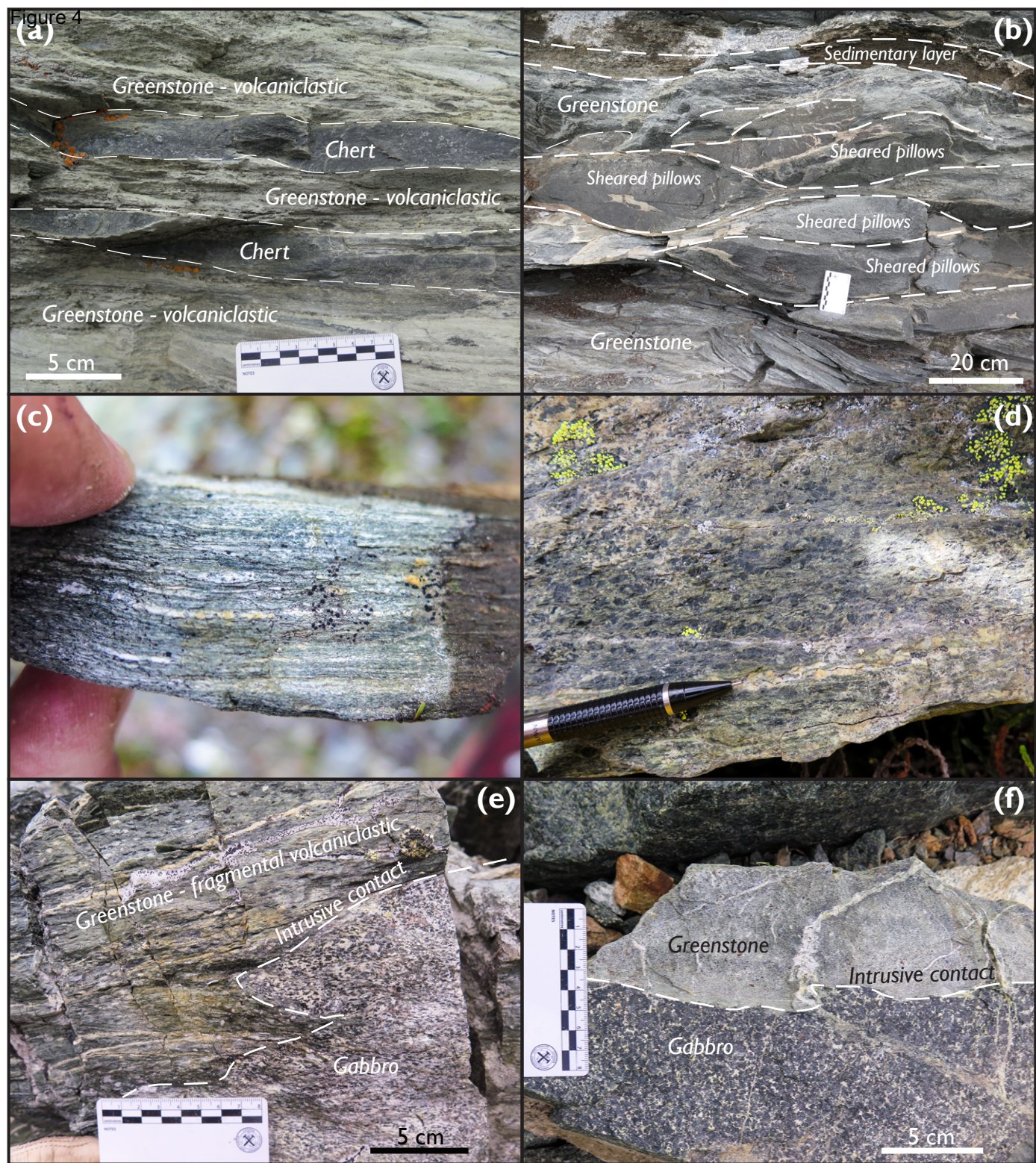


Figure 5

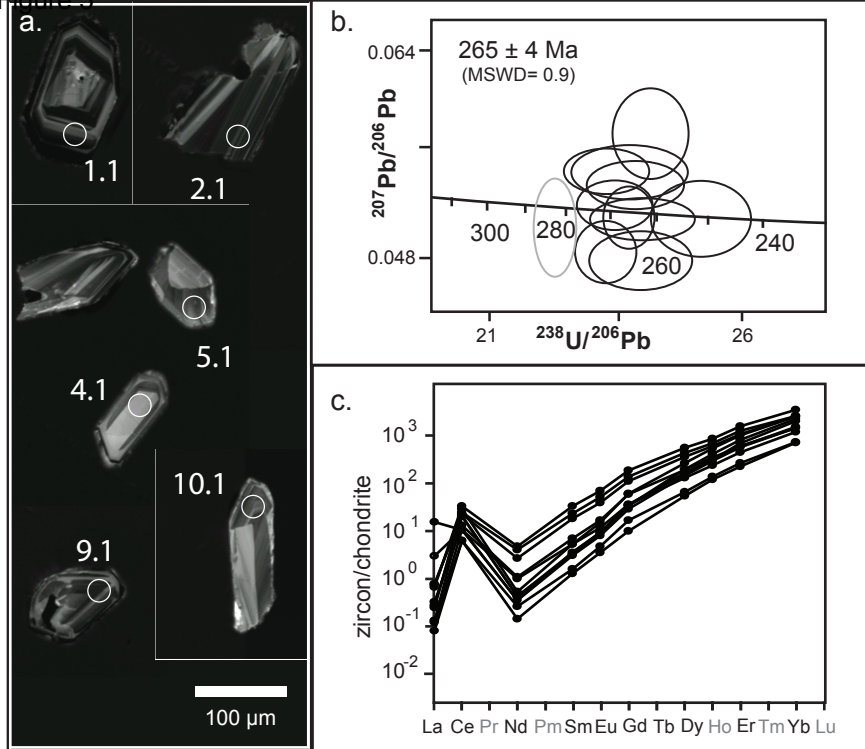


Figure 6

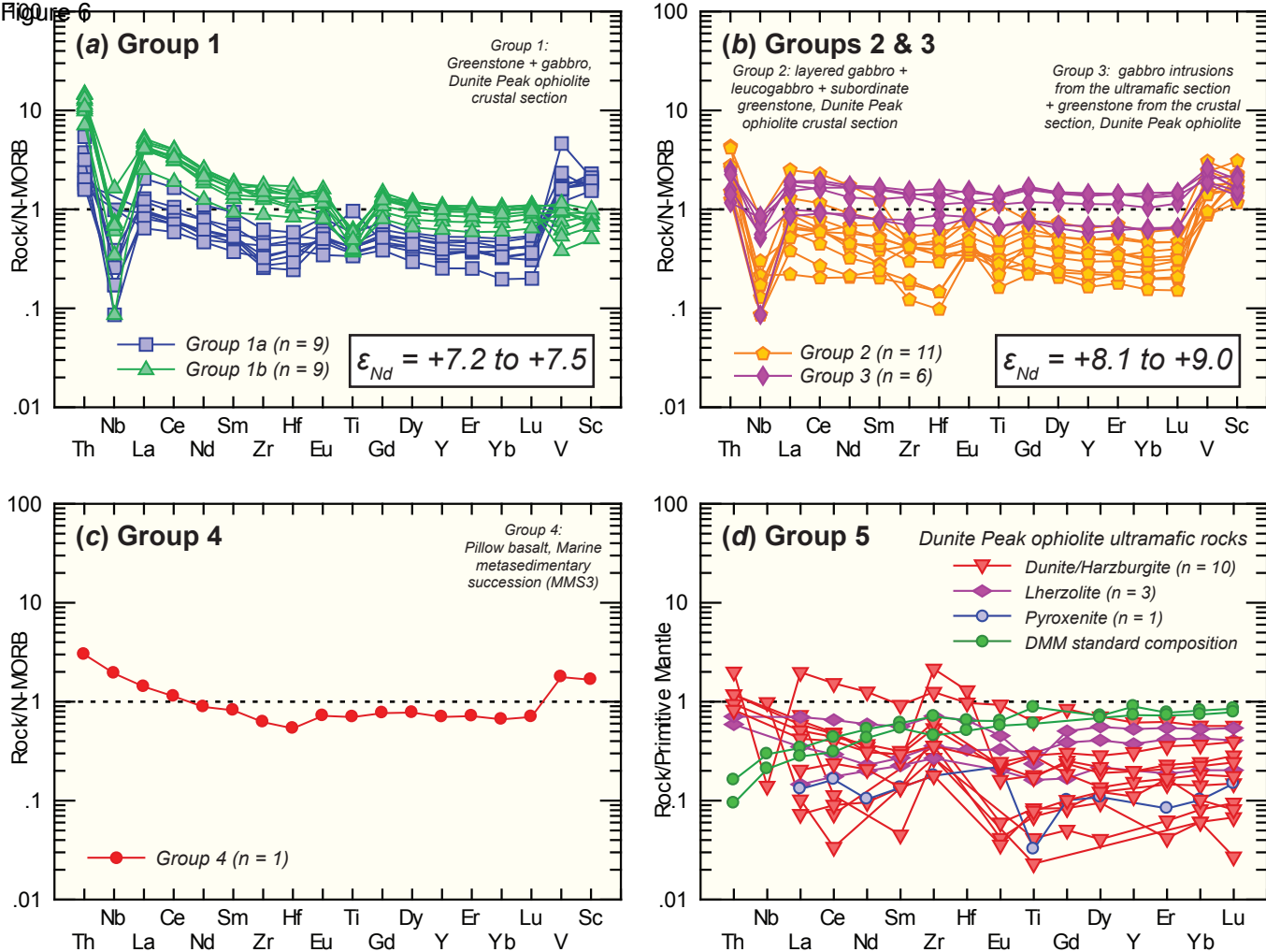


Figure 7

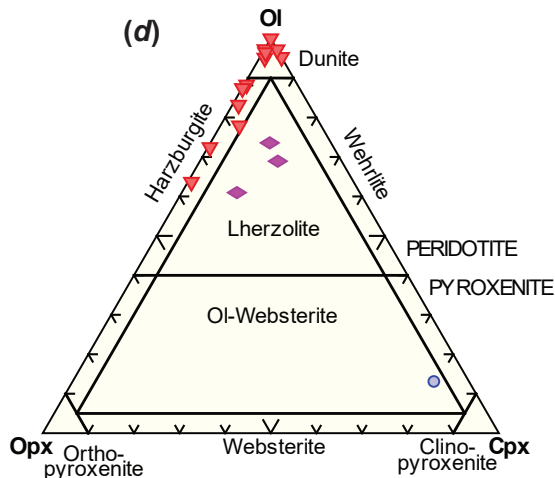
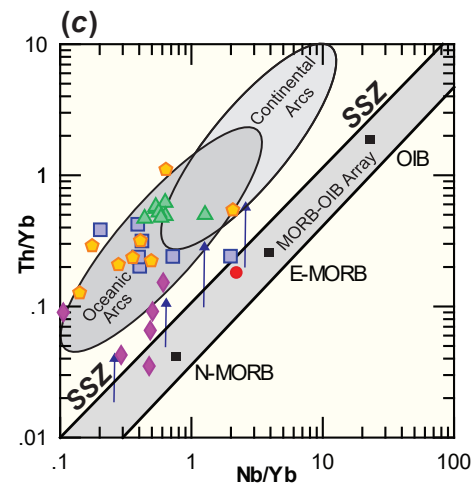
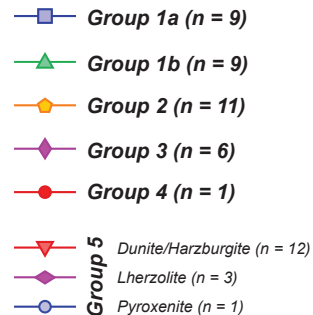
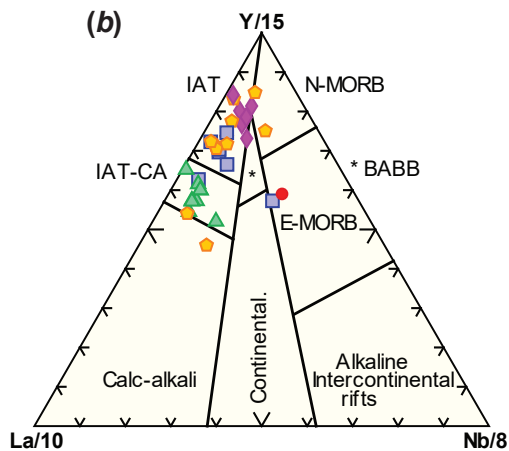
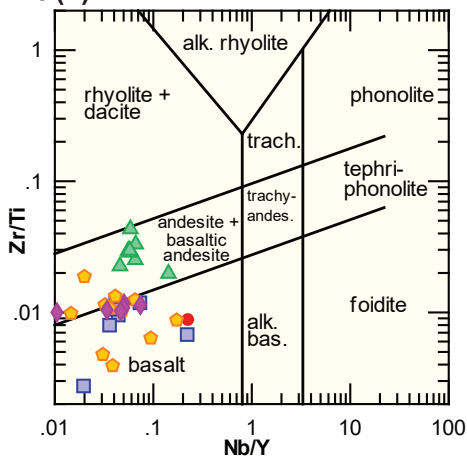
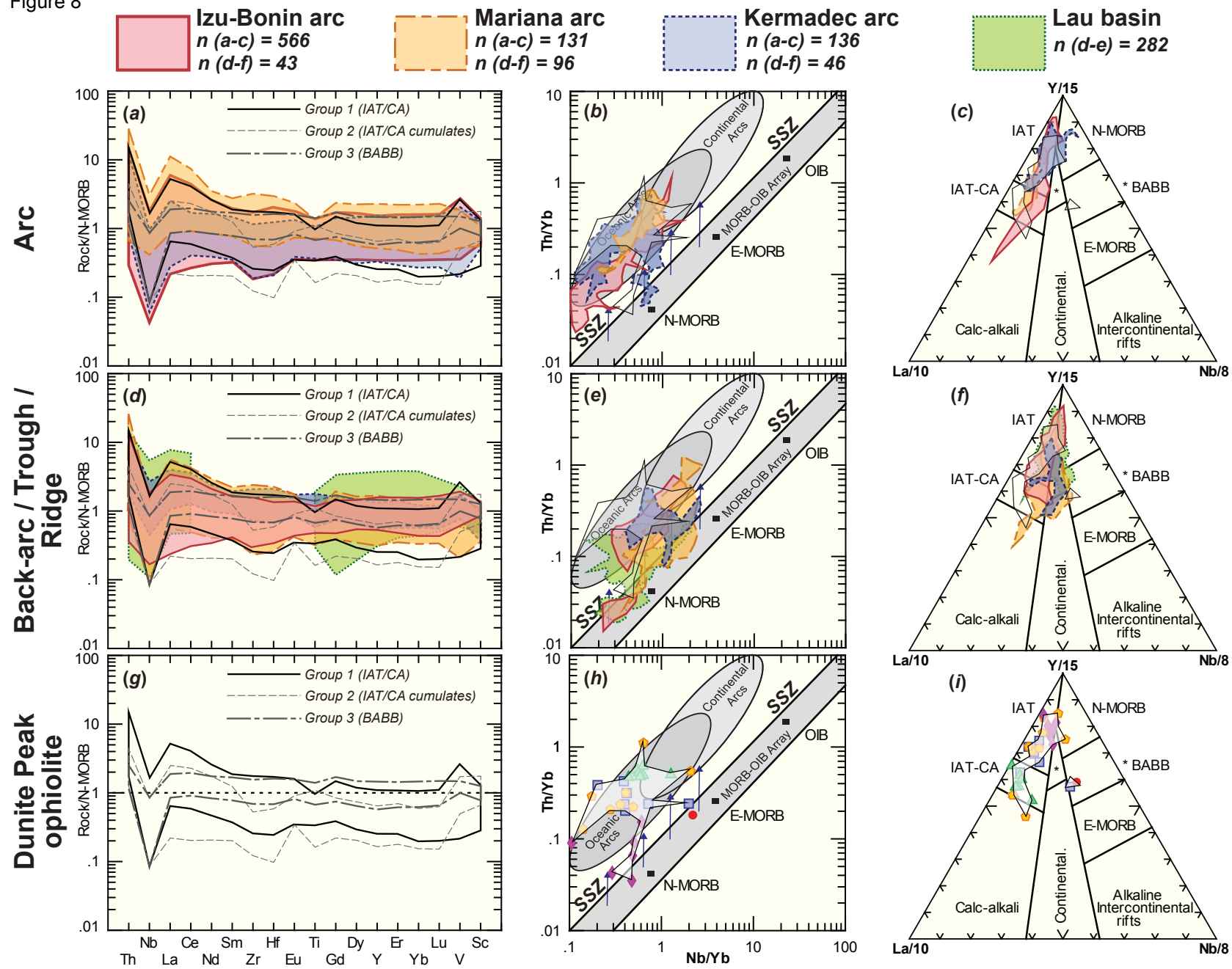
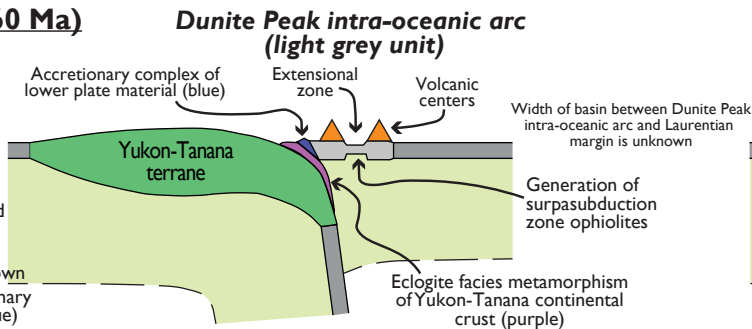


Figure 8



(a) Mid Permian (280-260 Ma)

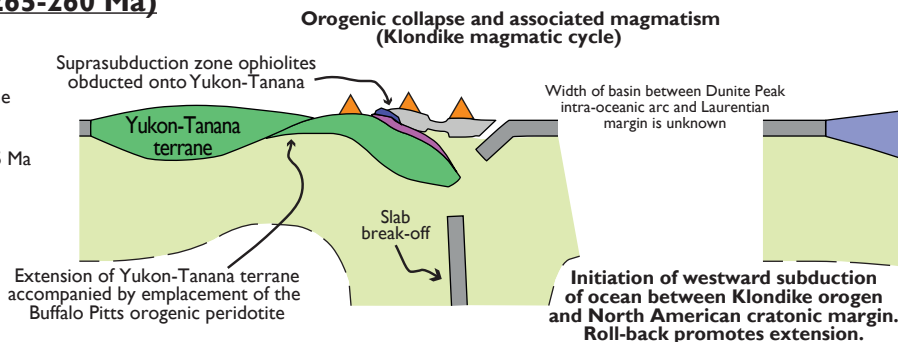
- Magmatism recorded by the Dunite Peak intra-oceanic arc between ~275 and 260 Ma and perhaps as early as ~280 Ma
- Eclogite facies metamorphism of Yukon-Tanana terrane recorded between ~275 and 260 Ma
- Late Permian and older parts of Slide Mountain terrane may represent accreted lower plate material from the subducted oceanic lithosphere (dark blue)
- Width of subducted ocean basin is unknown
- St Cyr blueschist may represent accretionary complex of lower plate material (dark blue)



Earliest record of eclogite facies metamorphism of Yukon-Tanana terrane marks start of the Klondike orogeny. Coeval Dunite Peak magmatism and eclogite facies metamorphism of Yukon-Tanana terrane suggests Yukon-Tanana had an irregular shape with promontories and re-entrants and/or collided obliquely with the Dunite Peak intra-oceanic arc. Co-spatial and coeval development of constructional volcanic centres (e.g. Dunite Peak, Wolf Mountain klippe) and zones of extensional volcanism (e.g. Sylvester allochthon, Finlayson Lake district) is comparable to disorganized extensional intra-oceanic arcs such as the Kermadec arc - Havre trough system

(b) Mid/late Permian (265-260 Ma)

- Cessation of Dunite Peak magmatism and subduction of Yukon-Tanana terrane by 260 Ma
- Exhumation of Yukon-Tanana terrane blueschists and eclogites initiated at 265 Ma
- Emplacement of Buffalo Pitts orogenic peridotite within Yukon-Tanana terrane at ~262 Ma
- Main phase of Klondike magmatic cycle between 265 and 252 Ma

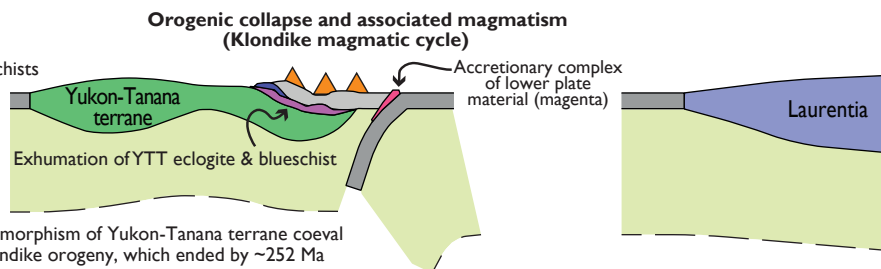


Buoyancy-driven slab break-off from the east margin of Yukon-Tanana terrane was followed by extension, exhumation and magmatism associated with orogenic collapse and initiation and roll-back of westward subduction beneath the Klondike orogen

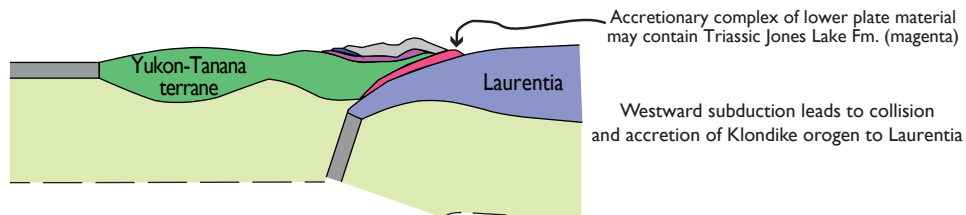
(c) Late Permian (260-252 Ma)

- Continued exhumation of Yukon-Tanana terrane blueschists and eclogites between 265 and 256 Ma
- Klondike magmatic cycle continued until 252 Ma
- Amphibolite facies metamorphism of Yukon-Tanana terrane recorded between ~260 and 252 Ma

Latest occurrence of Klondike magmatism and metamorphism of Yukon-Tanana terrane coeval with exhumation marks the final stages of the Klondike orogeny, which ended by ~252 Ma



(d) Post-Middle Triassic



- Collision and accretion of Klondike orogen to Laurentian margin facilitated by westward subduction of the ocean basin between the Klondike orogen and Laurentia
- Triassic clastic deposits of the Jones Lake Formation (magenta) may represent obducted lower plate sediments from the basin between the Klondike orogen and Laurentia
- Detrital zircons from the Jones Lake Formation suggest the Klondike orogen and Laurentian margin were in close proximity by the Late Triassic
- Late Triassic - Jurassic magmatism and Early Jurassic metamorphism recorded by Yukon-Tanana terrane are absent from Laurentia in Yukon
- Early Jurassic metamorphism and exhumation of Yukon-Tanana terrane records an Early Jurassic collisional event
- Early Cretaceous plutonic suites in Yukon-Tanana terrane and Laurentia indicate collision and accretion of Klondike orogen to Laurentian margin occurred by that time.
- Collision and accretion of Klondike orogen with Laurentian margin occurred after the Middle Triassic and by the Early Cretaceous

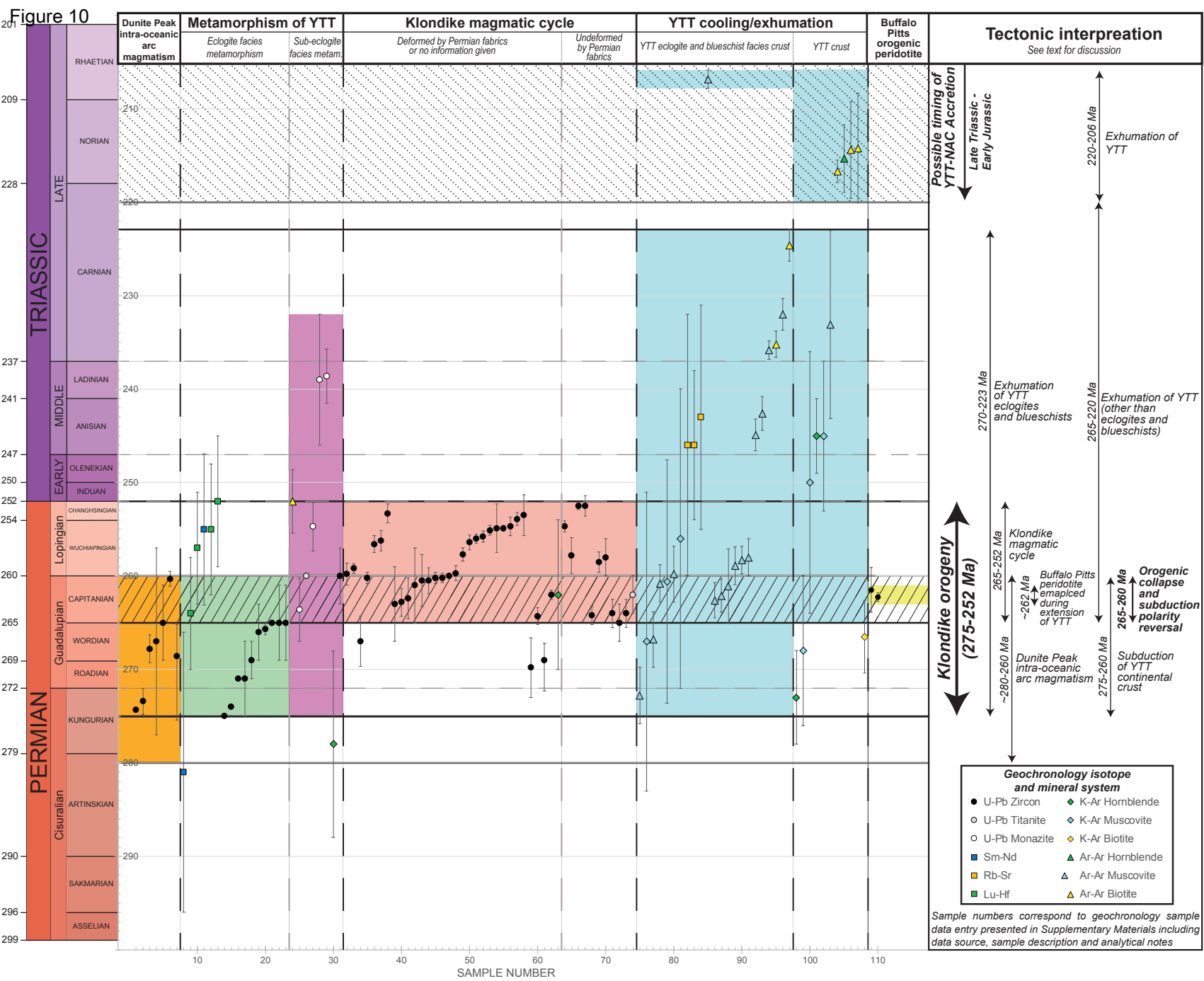


Table 1

| Sample | Group | Lithology | Map Unit | La _N ⁽¹⁾ | Mean La _N ⁽¹⁾ | Yb _N ⁽¹⁾ | Mean Yb _N ⁽¹⁾ | [La/Yb] _N ⁽¹⁾ | Mean [La/Yb] _N ⁽¹⁾ | [Th/Nb] _N ⁽¹⁾ | Mean [Th/Nb] _N ⁽¹⁾ | [V/Ti] _N ^(2,3) | Mean [V/Ti] _N ^(2,3) | ε _{Nd} ⁽⁴⁾ | Latitude | Longitude |
|---------------|-------|-------------------|----------|--------------------------------|-------------------------------------|--------------------------------|-------------------------------------|-------------------------------------|--|-------------------------------------|--|--------------------------------------|---|--------------------------------|-------------|--------------|
| 17RAY-AP034A1 | 1a | Greenstone | DP1 | 0.81 | 1.08 | 0.33 | 0.37 | 2.44 | 2.87 | 11.65 | 14.67 | 2.21 | 2.38 | | 61.63506654 | -134.0680117 |
| 17RAY-AP043B1 | 1a | Greenstone | DP1 | 0.64 | | 0.20 | | 3.27 | | - | | 1.99 | | | 61.59242971 | -134.0639359 |
| 15RAY-JR074A | 1a | Greenstone | DP1 | 1.20 | | 0.41 | | 2.93 | | 6.47 | | 2.36 | | 7.2 | 61.59007387 | -134.0590501 |
| 15RAY-JR076A | 1a | Greenstone | DP1 | 0.88 | | 0.32 | | 2.71 | | 9.71 | | 2.65 | | | 61.59540921 | -134.0717427 |
| 16RAY-AP074A2 | 1a | Greenstone | DP1 | 1.28 | | 0.47 | | 2.73 | | 14.56 | | 2.06 | | 7.4 | 61.63129486 | -133.9679625 |
| 16RAY-AP075A2 | 1a | Greenstone | DP1 | 0.92 | | 0.38 | | 2.42 | | 2.36 | | 2.86 | | 7.5 | 61.59011971 | -134.0590276 |
| 16RAY-AP076B1 | 1a | Greenstone | DP1 | 2.05 | | 0.50 | | 4.06 | | 21.03 | | 2.30 | | | 61.5836507 | -134.0376631 |
| 16RAY-AP088A1 | 1a | Greenstone | DP1 | 0.94 | | 0.32 | | 2.91 | | 36.89 | | 2.73 | | | 61.63073 | -133.96776 |
| 16RAY-JR111A2 | 1a | Greenstone | DP1 | 0.98 | | 0.41 | | 2.38 | | - | | 2.26 | | | 61.58143204 | -134.0379607 |
| 17RAY-AP035A2 | 1b | Greenstone | DP1 | 4.32 | 4.21 | 0.99 | 0.90 | 4.38 | 4.68 | 17.93 | 27.95 | 0.54 | 0.93 | | 61.63232538 | -134.0755242 |
| 17RAY-AP040A1 | 1b | Greenstone | DP1 | 4.12 | | 0.90 | | 4.60 | | 15.78 | | 0.61 | | | 61.58670054 | -134.0502722 |
| 16RAY-AP076A1 | 1b | Greenstone | DP1 | 4.00 | | 0.73 | | 5.50 | | 19.00 | | 1.15 | | | 61.5836507 | -134.0376631 |
| 16RAY-AP087B2 | 1b | Greenstone | DP1 | 4.64 | | 0.98 | | 4.72 | | 7.66 | | 0.84 | | 7.4 | 61.63234 | -133.97231 |
| 16RAY-AP104A1 | 1b | Greenstone | DP1 | 4.04 | | 0.83 | | 4.87 | | 15.05 | | 1.03 | | | 61.62589037 | -134.0045107 |
| 16RAY-AP159A1 | 1b | Greenstone | DP1 | 5.20 | | 1.04 | | 5.00 | | 20.10 | | 0.65 | | | 61.59755302 | -133.9073774 |
| 16RAY-AP181A1 | 1b | Gabbro | DP1 | 4.20 | | 1.07 | | 3.94 | | 114.56 | | 0.98 | | | 61.60605985 | -133.9014004 |
| 16RAY-AP209A1 | 1b | Greenstone | DP1 | 2.50 | | 0.60 | | 4.20 | | 20.63 | | 1.43 | | | 61.62199554 | -134.0470874 |
| 16RAY-AP234A1 | 1b | Greenstone | DP1 | 4.84 | | 0.98 | | 4.94 | | 20.87 | | 1.11 | | | 61.58258804 | -134.0346879 |
| 17RAY-AP041A1 | 2 | Greenstone | DP1 | 1.30 | 0.85 | 0.46 | 0.32 | 2.82 | 2.91 | 12.82 | 17.43 | 2.08 | 2.54 | | 61.58804837 | -134.0538744 |
| 17RAY-AP043A1 | 2 | Gabbro | DP1 | 0.67 | | 0.27 | | 2.53 | | 8.74 | | 2.83 | | | 61.59242971 | -134.0639359 |
| 17RAY-AP043C1 | 2 | Gabbro | DP1 | 0.52 | | 0.59 | | 0.87 | | - | | 1.56 | | | 61.59242971 | -134.0639359 |
| 17RAY-AP044A1 | 2 | Gabbro (cumulate) | DP1 | 2.50 | | 0.30 | | 8.27 | | 5.11 | | 2.82 | | | 61.59493771 | -134.0843975 |
| 16RAY-AP074A1 | 2 | Gabbro | DP1 | 0.92 | | 0.37 | | 2.46 | | 32.04 | | 2.46 | | | 61.63095953 | -133.9672315 |
| 16RAY-AP078C1 | 2 | Gabbro | DP1 | 0.89 | | 0.15 | | 5.79 | | 33.66 | | 4.22 | | | 61.59874752 | -133.9266214 |
| 16RAY-AP095A1 | 2 | Gabbro | DP1 | 0.60 | | 0.24 | | 2.52 | | 14.56 | | 3.19 | | | 61.62962702 | -133.9452507 |
| 16RAY-AP120B1 | 2 | Leucogabbro | DP1 | 0.22 | | 0.20 | | 1.12 | | - | | 1.85 | | | 61.59001219 | -133.9541316 |
| 16RAY-AP195A1 | 2 | Gabbro | DP1 | 0.74 | | 0.32 | | 2.32 | | 15.05 | | 1.56 | | | 61.59460302 | -133.9347754 |
| 16RAY-AP202A1 | 2 | Greenstone | DP1 | 0.64 | | 0.47 | | 1.37 | | 17.48 | | 2.08 | | | 61.58652204 | -134.0379319 |
| 16RAY-AP212B1 | 2 | Gabbro | DP1 | 0.38 | | 0.20 | | 1.90 | | - | | 3.24 | | | 61.61442871 | -134.050282 |
| 17RAY-AP041B1 | 3 | Greenstone | DP1 | 0.85 | 1.49 | 0.62 | 1.07 | 1.37 | 1.41 | 16.50 | 5.29 | 1.58 | 1.20 | | 61.58804837 | -134.0538744 |
| 17RAY-AP053A1 | 3 | Gabbro (cumulate) | DP2c | 1.92 | | 1.35 | | 1.42 | | 2.62 | | 1.06 | | | 61.61659902 | -133.9118072 |
| 16RAY-AP121B2 | 3 | Greenstone | DP1 | 1.76 | | 1.04 | | 1.69 | | 3.52 | | 1.17 | | | 61.59276702 | -133.9526361 |
| 16RAY-AP130C3 | 3 | Gabbro (cumulate) | DP2c | 1.54 | | 1.31 | | 1.17 | | 1.43 | | 0.84 | | 9.0 | 61.60996203 | -133.9634552 |
| 16RAY-AP179A1 | 3 | Greenstone | DP1 | 0.99 | | 0.65 | | 1.53 | | 4.85 | | 1.51 | | 8.3 | 61.60182918 | -133.9070494 |
| 16RAY-AP199A1 | 3 | Gabbro (cumulate) | DP2c | 1.88 | | 1.46 | | 1.29 | | 2.84 | | 1.03 | | 8.8 | 61.59690452 | -133.9366562 |
| 16RAY-AP079A1 | 4 | Pillow Basalt | MMS3 | 1.42 | 1.42 | 0.66 | 0.66 | 2.14 | 2.14 | 1.55 | 1.55 | 1.43 | 1.43 | | 61.62613451 | -133.8870414 |
| 15RAY-JR075A | 5 | Harzburgite | DP2b | - | 0.50 | 0.10 | 0.21 | - | 2.37 | - | 14.26 | - | 5.87 | | 61.60353936 | -133.9715166 |
| 16RAY-AP088D1 | 5 | Dunite | DP2b | 0.64 | | 0.18 | | 3.51 | | - | | 2.04 | | | 61.63073 | -133.96776 |
| 16RAY-AP093A1 | 5 | Dunite | DP2b | 0.58 | | 0.24 | | 2.39 | | - | | 4.00 | | | 61.62613 | -133.96498 |
| 16RAY-AP094A1 | 5 | Dunite | DP2b | - | | 0.04 | | - | | - | | 8.59 | | | 61.62751169 | -133.945937 |
| 16RAY-AP099A2 | 5 | Harzburgite | DP2b | 0.73 | | 0.08 | | 8.97 | | - | | 11.75 | | | 61.62295119 | -133.9497852 |
| 16RAY-AP101A1 | 5 | Lherzolite | DP2b | 0.35 | | 0.43 | | 0.82 | | - | | 2.80 | | | 61.6222022 | -133.993315 |
| 16RAY-AP113A2 | 5 | Harzburgite | DP2b | - | | 0.14 | | - | | - | | 8.46 | | | 61.61678803 | -133.994688 |
| 16RAY-AP123A2 | 5 | Dunite | DP2b | 0.10 | | 0.06 | | 1.67 | | - | | 7.40 | | | 61.60240819 | -133.9659106 |
| 16RAY-AP151A1 | 5 | Harzburgite | DP2b | 1.98 | | 0.57 | | 3.49 | | 14.26 | | 0.64 | | | 61.62396118 | -133.902718 |
| 16RAY-AP172A2 | 5 | Lherzolite | DP2b | 0.15 | | 0.20 | | 0.72 | | - | | 2.42 | | | 61.59975069 | -133.9312397 |
| 16RAY-AP172A1 | 5 | Lherzolite | DP2b | 0.70 | | 0.53 | | 1.32 | | - | | 2.02 | | | 61.59975069 | -133.9312397 |
| 16RAY-AP174A2 | 5 | Dunite | DP2b | 0.07 | | 0.06 | | 1.20 | | - | | 4.26 | | | 61.59814669 | -133.9385149 |
| 16RAY-AP178B1 | 5 | Pyroxenite | DP2b | 0.13 | | 0.10 | | 1.29 | | - | | 26.82 | | | 61.61149835 | -133.9274497 |
| 16RAY-AP196D1 | 5 | Dunite | DP2a | 0.51 | | 0.22 | | 2.28 | | - | | 1.57 | | | 61.59532635 | -133.9356914 |
| 16RAY-AP205A1 | 5 | Harzburgite | DP2a | 0.42 | | 0.37 | | 1.16 | | - | | 2.47 | | | 61.59274121 | -134.0641057 |
| 16RAY-AP206A1 | 5 | Harzburgite | DP2a | 0.20 | | 0.10 | | 2.01 | | - | | 2.80 | | | 61.59335037 | -134.064108 |

Footnotes

Full data set and QC presented in Supplementary Materials 02

- indicates no data, due to concentratons outside of detection limits

1) Normalized against standard N-MORB composition (Sun & McDonough, 1989), except Group 5, which is normalized against standard primitive mantle composition (Sun & McDonough, 1989)

2) Ti normalized against standard N-MORB composition (Sun & McDonough, 1989), except Group 5, which is normalized against primitive mantle composition (McDonough & Frey, 1989)

3) V normalized against standard N-MORB composition (Klein, 2004), except Group 5, which is normalized against primitive mantle composition (McDonough & Frey, 1989)

4) εNd calculation based on a model age of 265 Ma